ISSN 0915-633X

NATIONAL INSTITUTE FOR FUSION SCIENCE

Theory of Self-Sustained Turbulence in Confined Plasmas

K. Itoh, S-I. Itoh, A. Fukuyama and M. Yagi

(Received - Feb. 7, 1996)

NIFS-399 Feb. 1996

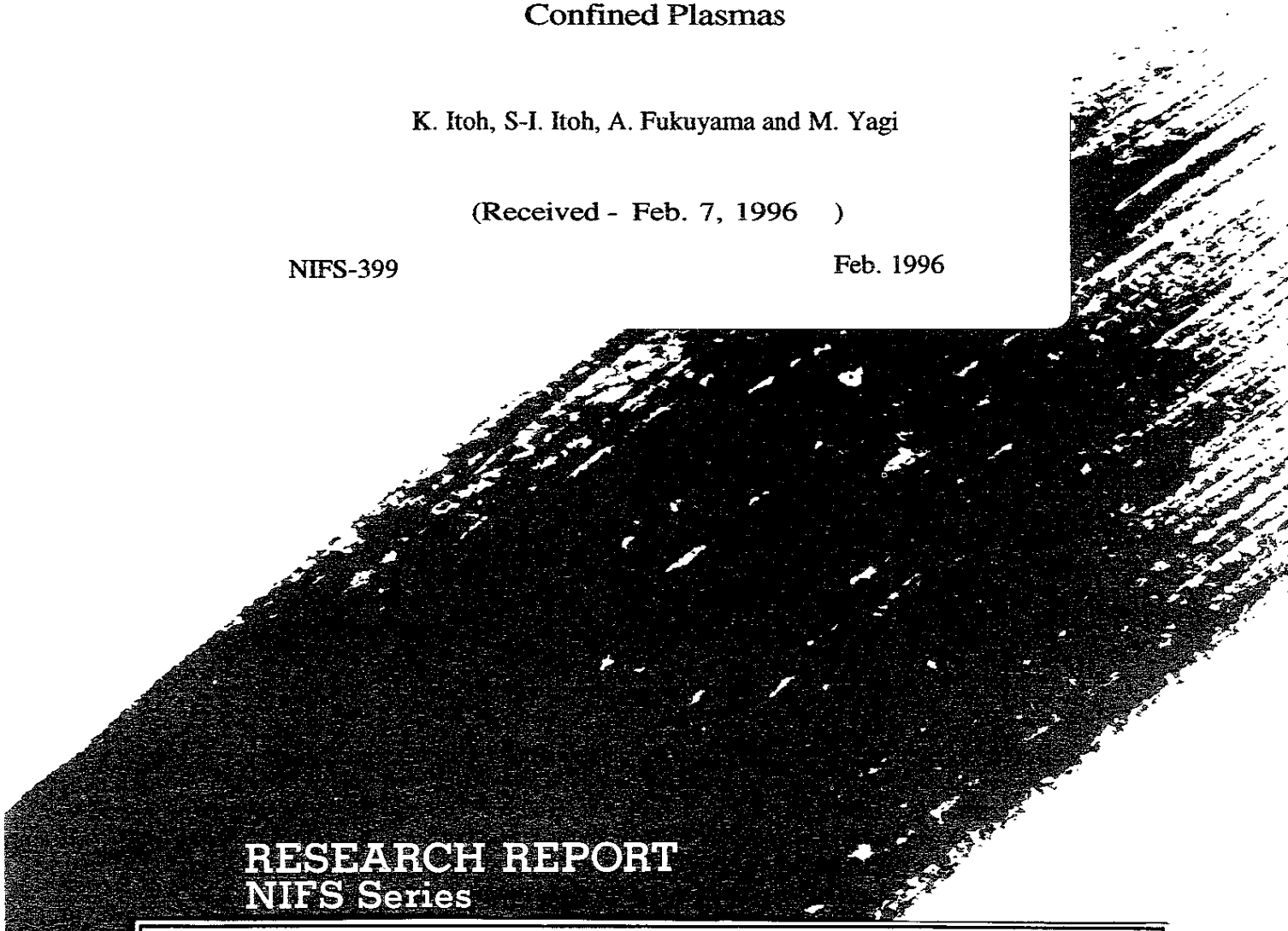

RESEARCH REPORT
NIFS Series

NAGOYA, JAPAN

Theory of Self-Sustained Turbulence in Confined Plasmas

Kimitaka Itoh*, Sanae-I. Itoh†, Atsushi Fukuyama**, Masatoshi Yagi†

* National Institute for Fusion Science, Nagoya 464-01, Japan

† Institute for Applied Mechanics, Kyushu University 87, Kasuga 816, Japan

** Faculty of Engineering, Okayama University, Okayama 700, Japan

This article is prepared for the special issue of Plasma Physics Reports.

Keywords: plasma turbulence, anomalous transport, bifurcation, structural formation, Self-sustained turbulence, radial electric field, improved confinement, simulation

Abstract

This article overviews some aspect of the recent theoretical activities in Japan on the problem of turbulent transport in confined plasmas. The method of self-sustained turbulence is discussed. The process of the renormalization is shown and the turbulent Prandtl number is introduced. Nonlinear destabilization by the electron momentum diffusion is explained. The nonlinear eigenmode equation is derived for the dressed-test-mode for the inhomogeneous plasma in the shear magnetic field. The eigenvalue equation is solved, and the least stable mode determines the anomalous transport coefficient. Formula of thermal conductivity is presented for the system of bad average magnetic curvature (current diffusive interchange mode (CDIM) turbulence) and that for the average good magnetic curvature (current diffusive ballooning mode (CDBM) turbulence). The transport coefficient, scale length of fluctuations and fluctuation level are shown to be the increasing function of the pressure gradient. Verification by use of the nonlinear simulation is shown. The bifurcation of the electric field and improved confinement is addressed, in order to explain the H-mode physics. Improved confinement and the dynamics such as ELMs are explained. Application to the transport analysis of tokamaks is also presented, including the explanations of the L-mode confinement, internal transport barrier as well as the role of current profile control.

1. Introduction

Plasma structure in confined plasmas has long been subject to intensive studies. Associated with this, the research on the theory of nonlinear interactions in plasmas has been motivated. There have been noticeable progresses in nonlinear plasma physics; the problem of solitons and that of plasma turbulence. Solitons has special relevance for plasmas, due to the intrinsic coupling between the plasma dynamics and the electromagnetic fields. The turbulence is also the key concept for the study of the confined plasmas. Dr. Petviasivili has left prominent steps both in these two directions of the nonlinear plasma theory. Those include, e.g., the foundation of the Kadomtsev-Petviasivili equation, which is one of the very few examples of integrable systems in higher dimensions, [1] or the investigation of the instability driven by plasma inhomogeneities [2]. In this article, we overview some aspect of the recent theoretical activities in Japan on the problem of turbulent transport in confined plasmas. (The scope of this article is not the worldwide review and references are far from exhaustive. An effort of review is given in [3], which supplements the material in this article.)

The anomalous transport has been known from the beginning of the fusion research [4]. Its origin is considered to be the low-frequency fluctuations, which are enhanced by plasma instabilities and give rise to the cross field transport. The theoretical task is to develop the methodology that allows to determine the fluctuation level and induced transport in the unstable plasmas. One of the established methods is called as the mixing-length-estimate, which balances the linear growth rate of the mode, γ_L, to the nonlinear stabilization by the back-ground turbulence, $\gamma_d \sim Dk_\perp^2$ (D being the cross-field diffusion coefficient) [4]. This theory gives an estimate $D \sim \gamma_L k_\perp^{-2}$, and the main theoretical study afterwards has been the precise determination of the linear growth rate in the complex plasma geometry [5]. The efforts have not been sufficient to explain the plasma transport phenomena [6], and a break-through for the methodology itself is necessary. It has also been known, either theoretically or by numerical simulations, that the plasma is possibly subject to nonlinear instabilities [7]. In order to develop a new methodology for the turbulent transport, we have recently

developed the theory of "self-sustained turbulence" in inhomogeneous plasmas [8]. The main concept is that the scattering of electrons by the back-ground fluctuations can cause the nonlinear growth of the mode, γ_{ng}, and the stationary turbulence is realized by the balance $\gamma_{ng} \sim \gamma_d$. The chained interaction of the mode growth and enhanced transport becomes important when we take into account the diffusion of perturbed current. The eigenmode equation for the dressed test mode is deduced by renormalizing the turbulence. By solving the marginal stability condition for the dressed test mode, we obtain the turbulence level as well as the transport coefficient. The stationary state is no longer near by the equilibrium, but is characterized by the subcritical excitation of the fluctuations.

This article is organized as follows. In section 2, the model equation and renormalization are given for the case of current diffusive interchange mode (CDIM). Stability of the dressed test mode and the turbulent-driven transport are shown in section 3. Analytic estimate is compared to numerical simulation in section 4. In the next section, the analysis is extended to the case with magnetic well, for which we analyzed the current diffusive ballooning mode (CDBM). The electric field bifurcation and the H-mode physics are discussed in section 6. These analysis are applicable to tokamaks, and some examples, e.g., L-mode and internal transport barrier are finally discussed in section 7. Summary and discussion is given in section 8.

2. Model Equation and Renormalization

2.1 Model Equations

We study the high-aspect-ratio, toroidal plasma with magnetic hill and strong magnetic shear. Such a case applies to the central region of tokamaks where q is below unity [9] or the configuration like torsatron/Heliotron [10]. The minor and major radii of the torus are given by a and R, respectively. We use the toroidal coordinate (r, θ, ζ). The reduced set of equations for the electrostatic potential ϕ, pressure p, and current J are employed [11]. The equation of motion:

$$\frac{\partial \nabla_\perp^2 \varphi}{\partial t} + [\varphi, \nabla_\perp^2 \varphi] = \nabla_\parallel J + (\Omega' \times \hat{\zeta}) \cdot \nabla p + \mu_{\perp c} \nabla_\perp^4 \varphi \qquad (1)$$

the Ohm's law:

$$\frac{\partial \Psi}{\partial t} = -\nabla_\parallel \varphi - \frac{1}{\xi}\left(\frac{\partial J}{\partial t} + [\varphi, J] \right) - \frac{J}{\sigma_c} + \lambda_c \nabla_\perp^2 J \qquad (2)$$

the energy balance equation:

$$\frac{\partial p}{\partial t} + [\varphi, p] = \chi_c \nabla_\perp^2 p \qquad (3)$$

constitute the set of basic equations. In these equations, the bracket [f,g] denotes the Poisson bracket, $[f, g] = (\nabla f \times \nabla g) \cdot \vec{b}$, ($\vec{b}$ is the unit vector along the field line), Ω' is the average curvature of the magnetic field, Ψ is the vector potential, $1/\xi$ denotes the finite electron inertia, $\xi = (a/\delta)^2 \equiv (a\omega_p/c)^2$, and $1/\sigma_c$ is the classical resistivity. The transport coefficients $\mu_{\perp c}$, λ_c, χ_c are the contributions from collisional diffusion and are the viscosity for the perpendicular momentum, the current diffusivity, and the thermal diffusivity , respectively. In writing Eqs.(1)-(3), the normalization for resistive MHD (magnetohydrodynamic) modes is employed:$(\varepsilon v_A/a)t \to t$, $r/a \to r$, $\varphi/(\varepsilon a v_A B_0) \to \varphi$, $\Psi/(\varepsilon a B_0) \to \Psi$, $J(a\mu_0/\varepsilon B_0) \to J$, $p(2\mu_0/\varepsilon B_0^2) \to p$, $\sigma_c^{-1}(\tau_{Ap}/\mu_0 a^2) \to \sigma_c^{-1}$, $\mu_\perp(\tau_{Ap}/a^2) \to \mu_\perp$, $\lambda(\tau_{Ap}/\mu_0 a^4) \to \lambda$, $\chi(\tau_{Ap}/a^2) \to \chi$ where ε is the inverse aspect ratio, a/R, v_A is the Alfven velocity, B_0 is the main magnetic field, and $\tau_{Ap} = R/v_A$.

This set of equations (1)-(3) is a simplified one, and the generalization which includes the dynamics of the parallel motion [12] has also been analyzed. The coupling with the parallel motion turns out to be the correction of the order of β [13], and is neglected here for the transparency of the argument. The finite gyro-radius effect and the electron pressure terms in Ohm's law are neglected. (These effects give correction of the order of ω_*/γ, γbeing the growth rate or the decorrelation rate of the mode. As is shown in [8], for the case of helical systems, we have the estimates ω_*/γ is O(1/10), showing that these effects are small.)

2.2 Renormalization

The nonlinear equations (1)-(3) are transformed to the equations for the test mode (denoted by k) in the presence of background fluctuations (denoted by k_1) by employing a renormalization. In the process of renormalization, the back-interaction of the driven mode (denoted by k_2) on the original test mode is kept. The E×B nonlinearity is taken into account. The detailed procedure was given in [8]. The driven mode is given as

$$U_2 = \frac{1}{K_2}\left\{-N_u - \frac{ik_{\parallel 2}}{\gamma_{j2}}N_j - \frac{iA_2\gamma_{v2}}{\Gamma_{vp2}}N_p\right\} \tag{4}$$

$$J_2 = \frac{1}{K_2}\left\{-\frac{ik_{\parallel 2}\xi}{\gamma_{j2}k_{\perp 2}^2}N_u - \left[\frac{K_2}{\gamma_{j2}} - \frac{\xi k_{\parallel 2}^2}{\gamma_{j2}^2 k_{\perp 2}^2}\right]N_j + \frac{\xi A_2\gamma_{v2}k_{\parallel 2}}{\gamma_{j2}k_{\perp 2}^2\Gamma_{vp2}}N_p\right\} \tag{5}$$

$$p_2 = \frac{1}{K_2}\left\{\frac{i\gamma_{v2}G_2}{\Gamma_{vp2}k_{\perp 2}^2}N_u - \frac{G_2\gamma_{v2}k_{\parallel 2}}{\Gamma_{vp2}\gamma_{j2}k_{\perp 2}^2}N_j - \frac{\gamma_{v2}}{\Gamma_{vp2}}\left[K_2 + \frac{G_2A_2\gamma_{v2}}{k_{\perp 2}^2\Gamma_{vp2}}\right]N_p\right\} \tag{6}$$

and

$$K_2 = \gamma_{u2} + \frac{k_{\parallel 2}^2}{k_{\perp 2}^2}\frac{\xi}{\gamma_{j2}} - \frac{A_2G_2}{\gamma_{p2}k_{\perp 2}^2} \tag{7}$$

where $\gamma_{u2} = \gamma(2) + \Gamma_{u2}$, $\gamma_{j2} = \gamma(2) + \Gamma_{j2}$, $\gamma_{p2} = \gamma(2) + \Gamma_{p2}$, $\gamma(2)$ is the eigenvalue of the k_2 mode, $\partial\{U_2, J_2, p_2\}/\partial t = \gamma(2)\{U_2, J_2, p_2\}$, Γ_{u2}, Γ_{j2} and Γ_{p2} denote the decorrelation rate of U_2, J_2, and p_2 by the back-ground turbulence, respectively. (Suffix 1 and 2 denotes the abbreviation for k_1 and k_2, respectively.) Other notation is: U is the vorticity, $U = -k_\perp^2\varphi$, $iA_2p_2 = (\Omega'\times\hat{\zeta})\cdot\nabla p_2$, $G_2 = k_{\theta 2}(dp_0/dr)$, p_0 is the equilibrium pressure profile, and the nonlinear interaction terms are defined as

$$N_u = [\varphi_1, U_k],\ N_j = [\varphi_1, J_k],\ N_p = [\varphi_1, p_k]. \tag{8}$$

2.3 Diffusion Approximation and Mean Field Approximation

The nonlinear contribution to the original test wave is obtained by calculating the back-interaction of the driven mode (k_2) with the background turbulence ($-k_1$). Such a contribution has the form as $\Sigma[\phi_{-1}, U_2]$ and is proportional to $\Sigma[\phi_{-1}, [\phi_1, U_k]]$. Making the assumption that the wavelength of the turbulence is much shorter than the scale length of the envelope of fluctuations, and that the convective momentum associated with the turbulence is small, the nonlinear terms can be expressed in the form of a diffusion matrix [8]. The simplification of the isotropic turbulence is made as

$$\langle|\partial\varphi_1/\partial r|^2\rangle \simeq \langle|\partial\varphi_1/r\partial\theta|^2\rangle \simeq \langle|k_{\perp 1}\varphi_1|^2\rangle/2 \quad . \tag{9}$$

Bracket < > means a spectrum average. Only the diagonal elements are kept in the following argument. With these approximations and assumptions, Eqs.(1)-(3) reduce to a set of linearlized equations for the dressed test wave as follows:
The equation of motion:

$$\frac{\partial\nabla_\perp^2\varphi}{\partial t} + [\varphi_0, \nabla_\perp^2\varphi] + (\mu_{\perp k} + \mu_{\perp c})\nabla_\perp^4\varphi = \nabla_\parallel J + (\Omega'\times\hat{\zeta})\cdot\nabla p \tag{10}$$

the Ohm's law:

$$\frac{\partial\Psi}{\partial t} = -\nabla_\parallel\varphi - \frac{1}{\xi}\left(\frac{\partial J}{\partial t} + [\varphi_0, J]\right) - \frac{J}{\sigma_c} + (\lambda_k + \lambda_c)\nabla_\perp^2 J \tag{11}$$

and the energy balance equation:

$$\frac{\partial p}{\partial t} + [\varphi_0, p] - (\chi_k + \chi_c)\nabla_\perp^2 p = -[\varphi, p_0] \tag{12}$$

where the suffix 0 denotes the equilibrium distribution, and the suffix k denoting the test wave is suppressed for simplicity.

The mean field approximation is employed to perform the stability analysis and obtain the transport coefficients and turbulence level. We approximate the constants $\{\mu_{\perp k}, \lambda_k, \chi_k\}$ by a set of turbulent driven diffusion coefficients $\{\mu_\perp, \lambda, \chi\}$. We have

$$\mu_\perp = \Sigma \frac{|k_{\perp 1}\varphi_1|^2}{2}\frac{1}{K_1} \tag{13}$$

$$\lambda = (\delta/a)^2\mu_e \tag{14}$$

$$\mu_e = \Sigma \frac{|k_{\perp 1}\varphi_1|^2}{2}\frac{1}{K_1}\frac{\gamma_{u1}}{\gamma_{j1}}\left[1 - \frac{A_1 G_1}{\gamma_{u1}\gamma_{p1}k_{\perp 1}^2}\right] \tag{15}$$

$$\chi = \Sigma \frac{|k_{\perp 1}\varphi_1|^2}{2}\frac{1}{K_1}\frac{\gamma_{u1}}{\gamma_{p1}}\left[1 + \frac{\xi k_{\parallel 1}^2}{k_{\perp 1}^2\gamma_{u1}\gamma_{j1}}\right] \tag{16}$$

and

$$K_1 = \gamma_{u1} + \frac{k_{\parallel 1}^2}{k_{\perp 1}^2}\frac{\xi}{\gamma_{j1}} - \frac{A_1 G_1}{\gamma_{p1}k_{\perp 1}^2} \quad . \tag{17}$$

In these expressions summation is taken over the background fluctuations, k_1. The coefficient μ_e is the electron viscosity.

3. Stability of Dressed Test Mode and Transport Coefficient

3.1 Eigenmode Equation

The renormalized equations are given as a linear form for the dressed test wave with diffusion coefficients $(\mu_\perp, \lambda, \chi)$. Eliminating J and p from the set of equations, we have

$$k_\parallel \frac{k_\perp^2}{\gamma\left(1+\xi^{-1}k_\perp^2\right) + \lambda k_\perp^4} k_\parallel \tilde{\varphi} + \left(\gamma + \mu_\perp k_\perp^2\right)k_\perp^2\tilde{\varphi} - \frac{k_\theta^2 G_0}{\gamma + \chi k_\perp^2}\tilde{\varphi} = 0 \quad . \tag{18}$$

The term G_0 denotes the driving term of the interchange instability ,

$$G_0 = -\Omega' \frac{dp_0}{dr} \tag{19}$$

showing that the combination of bad magnetic curvature and pressure gradient causes the instability [14]. Equation (18) is the eigenvalue equation for the dressed test wave. The collisional diffusion coefficients are suppressed for the simplicity.

It has been shown that the mode can be strongly destabilized by the current diffusivity. The asymptotic form of the growth rate, in the presence of small but finite nonlinear interactions, was given as [8,15]

$$\gamma \propto \lambda^{1/5} . \tag{20}$$

Even a weak turbulence easily influences the growth rate. The schematic picture for the growth rate vs the background fluctuations is shown in Fig.1. The marginal stability condition is determined by the balance between the nonlinear destabilization and nonlinear stabilization. The nonlinear stationary state is different from the conventional picture in which the linear growth balances the nonlinear damping.

3.2 Marginal Stability Condition

The marginal stability condition for the least stable mode determines the anomalous transport coefficient. We obtain the marginal stability condition by setting $\gamma = 0$ in Eq.(18). We solve this equation by the Fourier transformation, $\tilde{\varphi}(r,\theta,\zeta) = \sum_{m,n} \exp(im\theta - in\zeta) \int_{-\infty}^{\infty} dk \varphi_{mn}(k) \exp(ikx)$ The mode is microscopic, and the (m,n) component is localized near the relevant rational surface $r = r_s$ (x denotes the distance from the rational surface, $x = r - r_s$). The (m,n) modes are treated separately in Eq.(18), because Eq.(18) is linearlized for the dressed test wave. We solve each (m,n) component and suppress the suffix (m,n) unless necessary. In this subsection, the argument k is the radial mode number.

In the vicinity of the rational surface, the parallel mode number is expressed as $k_{\|} = k_\theta s q^{-1} x$ where s is the shear parameter

$$s = q^{-1} r (dq/dr) \tag{21}$$

and q is the safety factor. By employing the Fourier transformation, x is replaced by the operator i(d/dk). The eigenvalue equation is then given as

$$k_\theta^2 s^2 q^{-2} \frac{d}{dk} \frac{1}{\lambda k_\perp^2} \frac{d}{dk} \varphi(k) - \mu_\perp k_\perp^4 \varphi(k) + \frac{k_\theta^2 G_0}{\chi k_\perp^2} \varphi(k) = 0 \tag{22}$$

where the perpendicular wave number is given as $k_\perp^2 = k_\theta^2 + k^2$. The equation is now expressed in terms of a second order ordinary differential equation with respect to the radial mode number k.

As in the study of the ballooning mode turbulence in tokamaks [8,15], we use the approximation to neglect the first derivative, $d\phi/dx$. This approximation yields

$$\frac{d^2}{dk^2}\varphi - \frac{\lambda \mu_\perp q^2 k_\perp^6}{k_\theta^2 s^2}\varphi + \frac{\lambda}{\chi}\frac{q^2 G_0}{s^2}\varphi = 0 \tag{23}$$

from Eq.(22). We rewrite χ in the form

$$\chi = h \frac{q^2 G_0^{3/2}}{s^2} \frac{\lambda}{\chi} \left(\frac{\chi}{\mu_\perp} \right)^{1/2} \tag{24}$$

where h is a numerical coefficient to be determined by the eigenvalue equation Eq.(23) or Eq.(22). The maximum value of h gives the transport coefficient in the stationary turbulence. For simplicity, we introduce the normalized poloidal wave number as

$$b = k_\theta^2 \left(\frac{q^2 \lambda \mu_\perp}{s^2} \right)^{1/3} \tag{25}$$

and the normalized radial wave number as

$$z^2 = k^2\left(\frac{q^2\lambda\mu_\perp}{s^2}\right)^{1/3} \tag{26}$$

By using this normalization, the eigenvalue equation Eq.(23) is rewritten as

$$\frac{d^2\varphi}{dz^2} + \left\{\left(H - b^2\right) - 3bz^2 - 3z^4 - b^{-1}z^6\right\}\varphi = 0\,. \tag{27}$$

The eigenvalue H is related to the coefficient h as $h = H^{-3/2}$. Neglecting z^2 and z^4 as in [15], the eigenvalue equation Eq.(27) is solved by the WKB method as

$$\left(H - b^2\right)^{2/3} b^{1/6}\int_0^1 \sqrt{1 - y^6}\,dy = \frac{\pi}{4} \tag{28}$$

The eigenvalue H is a function of b (i.e., normalized poloidal mode number):

$$H = b^2 + Cb^{-1/4} \tag{29}$$

where the coefficient C is given as $C = \left(\frac{4}{\pi}\int_0^1 \sqrt{1-y^6}\,dy\right)^{-3/2}$.

Equation (29) indicates that the stability boundary (i.e., the level of anomalous transport to suppress the nonlinear instability) is dependent on the mode number, as is schematically shown in Fig.2. The eigenvalue H takes the minimum H* of $H^* = 9(C/8)^{8/9}$ at the mode number satisfying

$$b = b^* = (C/8)^{4/9}\,. \tag{30}$$

The least stable mode is specified by b*. The coefficient h in Eq.(24) is given as

$$h = H_*^{-3/2} = (16/27)C^{-4/3}. \tag{31}$$

3.3 Transport Coefficients

Using the stability boundary for the least stable mode, Eq.(31), we have the transport coefficient χ as

$$\chi \cong \frac{q^2 G_0^{3/2}}{s^2} \frac{\lambda}{\chi} \left(\frac{\chi}{\mu_\perp} \right)^{1/2} . \tag{32}$$

The renormalization relation of the fluctuations, Eq.(13), indicates that the fluctuation level is estimated as $\varphi/B \simeq \mu_\perp$, or

$$\frac{e\varphi}{T} \simeq \mu_\perp \frac{eB}{T} . \tag{33}$$

The result shows that the transport coefficient is a function of the Prandtl numbers, $\mu_e/\mu_\perp$ and $\chi/\mu_\perp$. The Prandtl numbers are found to be close to unity. For the case of interchange mode, they were given as [16]

$$\mu_e/\mu_\perp \simeq 2.3, \ \chi/\mu_\perp \simeq 2.0 . \tag{34}$$

Substituting these numbers for $\mu_e/\mu_\perp$ and $\chi/\mu_\perp$ into Eq.(32) and have the transport coefficient, in normalized form , as

$$\chi \simeq 1.6 \, q^2 s^{-2} G_0^{3/2} (c/a\omega_p)^2 . \tag{35}$$

The numerical coefficient is only an order of magnitude estimate given analytically. A careful numerical study of the variational equation has also shown the reduced numerical coefficient [17].

The transport coefficient is expressed in physics quantities as

$$\chi = F(\hat{r}) \left(\frac{d\beta}{dr} \right)^{3/2} \left(\frac{c}{\omega_p} \right)^2 \frac{v_A}{R} \tag{36-1}$$

$$F(\hat{r}) = 1.6\left(\frac{q(\hat{r})^2}{dq/d\hat{r}}\right)^2\left(\frac{R^2}{2a^2}\frac{d\Omega}{d\hat{r}}\right)^{3/2} \qquad (36\text{-}2)$$

where $\hat{r}$ is the normalized radius, r/a.

The result illustrates that the anomalous transport coefficient has the dimensional dependence $\delta^2 v_A/R$ and is multiplied by the beta-value, indicating the driving by the pressure gradient. The importance of the collisionless skin depth in the anomalous transport coefficient has been pointed out by Ohkawa [18], and similar conclusion has been derived based on the quasi-linear treatment [19]. Comparison with experiment has suggested that the scale length dictating transport seems to have a dependence like Debye length [20]. Our result verifies by use of the nonlinear turbulence theory that the collisionless skin depth plays an important role in the anomalous transport.

The coefficient F contains a numerical coefficient and a geometrical factor. In the limit of a high-aspect-ratio torsatron/Heliotron configuration, the magnetic structure is approximately described in terms of a Bessel function [21]. In such a case, an analytic estimate yields $\frac{d\Omega}{d\hat{r}} \cong \frac{m}{\ell}\left(\frac{a}{R}\right)^2\frac{1}{\hat{r}^2}\frac{d}{d\hat{r}}\left(\frac{\hat{r}^4}{q}\right)$, where m is the toroidal pitch number and ℓ is the polarity of the helical windings, respectively. This gives an analytic expression for the geometrical factor F as

$$F(\hat{r}) = 1.6\left(\frac{q(\hat{r})^2}{dq/d\hat{r}}\right)^2\left(\frac{m}{2\ell}\frac{1}{\hat{r}^2}\frac{d}{d\hat{r}}\left(\frac{\hat{r}^4}{q}\right)\right)^{3/2}. \qquad (37)$$

The important role of the magnetic shear is shown in the term F. As is widely known, magnetic shear is inevitable in a system with a magnetic hill. The anomalous transport coefficient is predicted to depend as s^{-2}. When the magnetic shear is weak, the transport coefficient becomes very large. This is in contrast to the case of tokamaks and stellarators which is presented later.

3.4 Implication to Experiments in Torsatron/Heliotron

The predictions of the theory are discussed, comparing with experimental results. Firstly, the dimensional dependence of χ is $[\chi] \propto [T]^{1.5}[R]^{-1}[B]^{-2}$ and is independent of that of density [n]. Secondly, the formula for χ includes the radial dependence of $(\beta'/n)^{3/2}$, not $T^{3/2}$, and predicts a larger transport coefficient near the edge. These are consistent with observations [22]. Figure 3 illustrates a typical example of the radial profile of the predicted thermal diffusivity. Third, the thermal diffusivity which is deduced from heat pulse propagation, χ_{HP}, can be larger than the thermal diffusivity in the steady state. If the density profile is much flatter than that of the temperature, and if only the temperature is modulated by the heat pulse, the theoretical formula of χ gives the relation

$$\chi_{HP} \simeq 2.5\,\chi. \tag{38}$$

The theory predicts that the ion viscosity is also enhanced to the level of the thermal diffusivity. Anomalous ion shear viscosity has been observed recently in the CHS device, and the relation $\mu_{\parallel} \simeq \chi$ was observed [23]. This observation is consistent with theory [13].

The point model analysis gives the energy transport scaling law as

$$\tau_E \propto A_i^{0.2} B^{0.8} n^{0.6} a^2 R P^{-0.6} \langle F \rangle^{-0.4} \tag{39}$$

where A_i is the ion mass number, P is the heating power and <F> is the average of F near the boundary. The improvement of the confinement due to the increase of the shear (s^{-2} term in F) is almost completely offset by the increment of the magnetic hill Ω'. The coefficient F depends weakly on geometrical parameters such as pitch numbers. This result may explain the fact that τ_E seems to depend only weakly on the rotational transform or on the magnetic shear in the experimental data. The predicted indices for B, n, a, R and P, as a whole, are consistent with the experimental scaling law [22]. When the magnetic axis is shifted inward or outward, by applying the

vertical field, the magnetic shear and well change. Competition between the changes in shear and well is discussed in [13]. The inward shift of the magnetic axis, as a whole, can be favourable in reducing the anomalous transport in toroidal helical systems.

We finally note the characteristics of the fluctuations. The relation between the density perturbation and the potential perturbation was calculated from the relation $\tilde{n}/n \simeq (\omega_*/\gamma)e\phi/T$, giving

$$\frac{\tilde{n}}{n} \simeq \left(\frac{3|q'|}{q\bar{G}_0}\frac{\beta(a)R}{L_n}\right)\frac{e\phi}{T} \tag{40}$$

where L_n is defined as $n'/n = -1/L_n$ and $\bar{G}_0 = -(R^2/2a^2)(d\beta/d\hat{r})(d\Omega/d\hat{r})$. For the case of the Heliotron-E plasma, $\bar{G}_0 \simeq 60a\beta(0)/L_p$ and $q'/q \approx 4$ hold (L_p being the pressure gradient scale length), and we have $\frac{\tilde{n}}{n} \simeq \left(\frac{2L_p}{L_n}\frac{\beta(a)}{\beta(0)}\right)\frac{e\phi}{T}$. The term in the bracket is order 1/10, showing that the density fluctuation is smaller than the potential fluctuation. (This supports the neglect of the ω_* term in the equation of motion.) Fluctuation measurements in high power heating experiments have shown that $\tilde{n}/n$ is smaller than $e\phi/T$ [24], which is consistent with the theory.

4. Numerical Simulation

In this section, we report the nonlinear simulation of the current diffusive interchange mode by keeping the electron nonlinearity, i.e., the $E\times B$ nonlinear term in the Ohm's law [25,26]. We start from the three filed reduced set of equations (1)-(3) in a shear slab plasma with bad averaged curvature. The pressure gradient is taken in the x-direction, and main magnetic field is in the z-direction. In the slab geometry, the shear parameter s is taken into account as $k_{\|} = k_y sx$ and the origin x=0 is taken at the mode rational surface. The two-dimensional simulation is done and $\partial/\partial z = 0$. The back-ground modification, i.e., the change of the k_y=0 component, is omitted in this simulation, in order to study the physics of the self-sustained turbulence. In the

nonlinear simulation, the length and time are normalized to the collisionless skin depth $\delta = c/\omega_p$ and the poloidal Alfven transit time.

This system contains the linear interchange instability. In the limit of $\mu_c = \lambda_c = \chi_c = 0$, the linear growth rate γ_L is given as

$$\gamma_L = -s/2k_y + \sqrt{(s/2k_y)^2 + G_0}. \qquad (41)$$

The parameter G_0 represents the driving source, which is the product of the pressure gradient and bad magnetic curvature. When the ion viscosity and thermal conductivity are finite, both the longer-wave-length modes and the shorter-wave-length modes are stabilized. If μ_c and χ_c becomes larger, all the modes become linearly stable. For the set of parameters $\mu_c = \chi_c = 0.2$ and $\lambda_c = 0.01$ and $s = G_0 = 0.5$, the linear instability appears in the range of $0.2 < k_y < 0.9$ and the maximum linear growth rate is given as $\gamma_L \sim 0.17$ for $k_y \sim 0.5$. As the driving source decreases, the largest growth rate becomes smaller. As is shown in Fig.4, all the mode becomes linearly stable for the parameter of $G_0 < 0.4$.

Nonlinear simulation is performed by directly solving Eqs.(1)-(3) in the slab geometry of the system size of L =80 in the x-direction and L_y=6.4 in the y-direction. The periodicity condition is taken in the y-direction, and M=64 modes are taken in k_y-space ($k_{y,min} = 10/64$ and $k_{y,max} = 10$). The $\partial\Psi/\partial t$ term and the resistivity in the Ohm's law Eq.(2) are neglected to illuminate the transparency of the nonlinear mechanism of the instability. In evaluating the fluctuations, we define the fluctuation spectrums in the electric field, W_ϕ, the current, W_j, and the pressure, W_p, as $W_\phi(k_y) = [\int_0^L dx|\nabla_\perp\phi(x,k_y)|^2]/2L$, $W_j(k_y) = [\int_0^L dx|j(x,k_y)|^2]/2L$ and $W_p(k_y) = [\int_0^L dx|p(x,k_y)|^2]/2L$, respectively. The fluctuation levels are expressed by $<W_\phi>$, $<W_j>$ and $<W_p>$, where the average $<>$ denotes summation over poloidal mode numbers, as $<W_p> = \Sigma\, W_p(k_y)$. The energy conservation law is derived from as

$$\frac{\partial}{\partial t}(\langle W_\phi \rangle + \langle W_j \rangle + \langle W_p \rangle)$$
$$= (G_0 + 1)\Gamma - \langle \mu_c |\nabla_\perp^2 \phi|^2 \rangle - \langle \lambda_c |\nabla_\perp j|^2 \rangle - \langle \chi_c |\nabla_\perp p|^2 \rangle \qquad (42)$$

where $\Gamma = -\langle ik_y p^* \phi \rangle$ denotes the average energy flux in the direction of pressure gradient. This relation suggests that the stationary state is realized by the balance between the energy released by the plasma expansion and dissipation via collisional damping. The nonlinearlities, $[\phi,]$, transfer the wave energy between different modes and act as the effective diffusion in the phase space, but the real dissipation occurs through collisional transport.

Figure 5 shows the temporal evolution and nonlinear growth of fluctuations (solid line). In the small amplitude limit, the perturbations grows following the linear growth rate. However, at the time of $t \approx 35$, when the amplitude exceeds a certain threshold value, $\langle W_\phi \rangle \sim 10^{-4}$, the growth rate starts to increase. In the time range of $35 < t < 50$, the growth rate becomes larger as the amplitude increases. This is the nonlinear destabilization thorough the electron dynamics. The dashed line shows the result of reference simulation, in which the $[\varphi, j]$ term in Eq.(2) is omitted. (This reference case is called as "linear-Ohm's law" for abbreviation in this article.) In the case linear Ohm's law, the linear growth and nonlinear stabilization are observed, confirming the conventional picture of nonlinear stabilization.

The level of fluctuations for the nonlinear growth is compared to the theory. The current diffusivity, λ_N is estimated as $\lambda_N \simeq \sqrt{\langle W_\phi \rangle}/k_y$. For the value of $\langle W_\phi \rangle = 10^{-4}$ and $k_y = 0.6$, λ_N is estimated as 1.5×10^{-2} and becomes larger than λ_c. The growth rate, estimated by $\lambda = \lambda_N + \lambda_c$, is noticeably deviates from the linear estimation. The one-point renormalization in the theory gives a good approximation on the transition from the linear growth to the nonlinear instability.

The simulation in the longer time scale shows is shown in Figure 6. At the time of $t \sim 80$, the inverse cascade takes place, and the level shows transient dip. When t exceeds 100, the saturated state is realized. The dashed line (b) shows the reference case of linear Ohm's law (other parameters are common). The saturation level is

smaller in the case of linear Ohm's law. The case of increased λ_c ($\lambda_c = 0.2$) is shown by the line (c). For this large value, the linear growth rate becomes about twice larger and the change in the $k_\perp$ of the peak growth rate is less than 20%. Comparing the result of (a) and (c), we see that the saturation level is not sensitive to the linear growth rate in the current-diffusive interchange mode turbulence.

This insensitivity of the turbulence level becomes more prominent by calculating the linearly stable case. If G_0 is reduced to 0.3 and other parameters are fixed, all the modes becomes linearly stable (as is shown in Fig.4). In this case, growth of fluctuation occurs in the system of the nonlinear Ohm's law: When the initial amplitude is below the threshold value, the system remains stable and the fluctuation level does not increase. If, on the contrary, the initial condition exceeds the threshold value, the fluctuations start to grow and approaches a very high level, which is close to those for the linearly-*unstable* cases. The fluctuation level as a function of the pressure gradient is summarized in Fig.7. The linear growth rate is realized only in the very low level of initial amplitude (about 10^{-3} or less than the saturation level). The dynamical evolution of the fluctuations are governed by the nonlinear growth; the growth rate depends on the fluctuation level as is illustrated in Fig.1. The nonlinear simulation confirms the dependence of the saturation level as a function of the pressure gradient. In the previous section it is shown that the static potential fluctuation depends like $\varphi \propto G_0^{3/2}$, and the typical scale length of fluctuations behaves as $\langle k_\theta \rangle \propto G_0^{-1/2}$. This indicates the dependence of the electric field energy $<W_\phi>$, which is in proportion to $\varphi^2 k_\theta^2$, has a dependence

$$\langle W_\phi \rangle \propto G_0^2 \ . \tag{43}$$

The nonlinear simulation confirms the feature of the subcritical turbulence of the inhomogeneous plasmas.

The spectrum of the fluctuations is studied. The nonlinear growth takes place in the range of $k_y \sim 0.6$, and the spectrum extends to the higher mode numbers. This

extension is characteristic to the nonlinear Ohm's law. In the stationary stage, the largest amplitude mode is observed in the longer wave length mode. This is due to the inverse cascade from the nonlinearly excited modes of $k_y \sim 0.6$. In the region of $0.3 < k_y < 1.5$, the spectrum is fitted to

$$W_\phi(k_y) \propto k_y^{-3} \quad . \tag{44}$$

Above $k_y > 2$, the collisional dissipation dominates and W_ϕ is cut-off as $W_\phi(k_y) \propto \exp(-k_y)$.

The turbulent-driven energy flux is computed and is compared to the theoretical prediction. Since the simulation is done in the 2D model, the associated flux is localized in the vicinity of the rational surface. We define the localization width L_x by the condition $\bar{q} > 0.1\, \bar{q}_{max}$ for $|x| = L_x$, where $\bar{q} > L_y^{-1}\int_0^{L_y} dy\, q$, and $q = -ik_y p^*\phi$. The average turbulent driven flux $<q>$ is defined by $<q> = L_x^{-1}\int_0^{L_x} dx\, \bar{q}$. In the saturation stage, the time average in range of $100 < t < 200$ is about $\chi_{turb} = 3.0$ for the standard parameters ($s=0.5$, $G_0=0.5$). The theory predicts $\chi_N = G_0^{3/2}s^{-2}$, i.e., $\chi_N = \sqrt{2}$ for this set of parameters. Both the conductivity is much larger than the collisional transport coefficient χ_c.

The largest amplitude mode is found in the longer wave length modes. In this particular study, the largest amplitude mode is given for $k_y = 10/64$. This suggests that the wave length of peak of the spectrum is much longer than the collisionless skin depth, though the nonlinear interaction in the range of $k_y \sim 1$ causes the nonlinear growth and higher saturation. The inverse cascade has been observed in previous work [27]: For instance, the simulations on η_i mode turbulence has shown the inverse cascade, and the saturation level was found to be the level just after the inverse cascade takes place dominantly [26]. On the contrary, in the case of this simulation, the increase of the turbulence energy takes place once again after the prominent inverse cascade occurs.

5. Study of Current-Diffusive Ballooning Mode (CDBM) Turbulence

5.1 Application to the System with Magnetic Shear

The theory of the self-sustained turbulence and anomalous transport is extended to the system with magnetic shear (such as tokamaks and stellarators). In such geometry, the interchange mode remain stable, and we must analyze the ballooning mode, which is localized in the region of local bad magnetic curvature.

We take the high-aspect ratio limit of circular tokamaks. The ballooning transformation from the (r, θ) coordinates to the η coordinate [28] is employed, since we analyze the microscopic modes. By the help of the ballooning transform, the equation of the dressed test mode Eqs.(10)-(12) can be written in a form of the ordinary differential equation. The dispersion relation for the microscopic ballooning mode is given in the presence of turbulence as [8,15]

$$\frac{d}{d\eta}\frac{F}{\hat{\gamma}+\Xi F+\Lambda F^2}\frac{d\varphi}{d\eta}+\frac{\alpha[\kappa+\cos\eta+(s\eta-\alpha\sin\eta)\sin\eta]\varphi}{\hat{\gamma}+XF}-(\hat{\gamma}+MF)F\varphi=0 \qquad (45)$$

Terms Λ, X, and M represents the impact of the renormalized turbulence as $\Lambda=\hat{\lambda}n^4q^4$, $X=\hat{\chi}n^2q^2$ and $M=\hat{\mu}n^2q^2$. Ξ stands for the influence of the resistivity, $\Xi=n^2q^2/\hat{\sigma}$. Here normalization is used as $r/a\to\hat{r}$, $t/\tau_{Ap}\to\hat{t}$, $\chi\tau_{Ap}/a^2\to\hat{\chi}$, $\mu_\perp\tau_{Ap}/a^2\to\hat{\mu}$, $\lambda\tau_{Ap}/\mu_0a^4\to\hat{\lambda}$, $\tau_{Ap}/\sigma\mu_0a^2\to 1/\hat{\sigma}$ and $\gamma\tau_{Ap}\to\hat{\gamma}$. τ_{Ap} is the poloidal Alfven velocity $\tau_{Ap}=a\sqrt{\mu_0m_in_i}/B_p$, B_p is the poloidal magnetic field Br/qR, ε=r/R, $\beta=\mu_0n_i(T_e+T_i)/B^2$, s=r(dq/dr)/q, $\kappa=-\varepsilon(1-1/q^2)$, $F=1+(s\eta-\alpha\sin\eta)^2$, and $\alpha=-q^2R\beta'$ denotes the normalized pressure gradient. If one neglects the anomalous transport coefficient, Eq.(45) reduces to that for the resistive ballooning mode, and the ideal MHD mode equation [28] is obtained by taking $1/\sigma=0$.

5.2 Nonlinear Marginal Stability and Anomalous Transport Coefficient

Equation (45) constitutes the nonlinear dispersion relation. In the small amplitude limit, this dispersion relation describes the nonlinear instability driven by the anomalous current diffusion. An analytic estimate is given

$$\hat{\gamma} \sim \hat{\lambda}^{1/5}(nq)^{4/5}\alpha^{3/5}s^{-2/5} \tag{46}$$

showing that even the small amount of the current diffusivity can give a large nonlinear growth rate [8,15], as is illustrated in Fig.1.

The stationary state which satisfy the marginally stability condition (γ=0) gives the relation between the transport coefficients. In the case that the normal curvature is stronger than the geodesic curvature, $1/2+\alpha > s.$, Eq.(45) can be approximated as

$$\frac{d^2\phi}{d\eta^2} + \frac{\alpha\hat{\lambda}n^2q^2}{\hat{\chi}}\left(1-\left(\frac{1}{2}+\alpha-s\right)\eta^2\right)\phi - \hat{\mu}\hat{\lambda}n^6q^6\left(1+3(a-s)^2\eta^2\right)\phi = 0\,. \tag{47}$$

This equation gives the marginal stability condition as

$$\alpha^{3/2}\hat{\lambda}\hat{\chi}^{-3/2}\hat{\mu}^{-1/2} = f_1(N) \tag{48}$$

where the function f_1 and normalized mode number are defined as

$$f_1(N) = N^{-2}\left(1-N^4\right)^{-2}\left\{\frac{1}{2}+\alpha-s+3(\alpha-s)^2N^4\right\}, \tag{49-1}$$

$$N = nq(\hat{\chi}\hat{\mu}/\alpha)^{1/4}\,. \tag{49-2}$$

Equation (49-1) indicates that the level of anomalous transport, which causes the nonlinear stabilization, is dependent on the mode number, N. We see that the function $f_1(N)$ takes the minimum value $f(s,\alpha)$ at $N = N_*$, where

$$f(s,\alpha) = (1+2\alpha-2s)\sqrt{2+\frac{6(s-\alpha)^2}{1+2\alpha-2s}} \tag{50-1}$$

$$N_*^{-2} = \sqrt{2+6(s-\alpha)^2/(1+2\alpha-2s)}\,. \tag{50-2}$$

Substituting this result for the least stable mode, $N = N_*$, we have the expression of the anomalous transport coefficient as

$$\hat{\chi} = \frac{\alpha^{3/2}}{f(s,\alpha)} \frac{\hat{\lambda}}{\hat{\chi}} \sqrt{\frac{\hat{\chi}}{\hat{\mu}}} \tag{51}$$

where the coefficient $f(s,\alpha)$ represents the influence of the magnetic shear.

We here again note the fact that the Prandtl numbers, μ/χ and μ_e/χ, do not change much, compared to the magnitude of the transport coefficients itself, when the turbulence level is varied [16]. Taking the assumption that $\mu/\chi = 1$ and $\mu_e/\chi = 1$ hold, a simpler form of the anomalous transport coefficient is given From Eq.(51) as $\hat{\chi} = f(s,\alpha)^{-1}\alpha^{3/2}(c/a\omega_p)^2$, or in the dimensional form as

$$\chi = \frac{q^2}{f(s,\alpha)}(-R\beta')^{3/2}\left(\frac{c}{\omega_p}\right)^2 \frac{v_A}{R} \quad . \tag{52}$$

The function f is fitted as $0.4\sqrt{s}$ in the strong shear limit, and approximated as Eq.(50-1) in the weak shear limit. Figure 8 illustrates the dependence of the anomalous transport coefficient on the magnetic shear. This form of χ is consistent in various aspect of the L-mode transport. Detailed comparison by use of the transport code is explained in section 7.

The dominant role of current diffusive term in the Ohm's law in exciting turbulence indicates the relation $\hat{\lambda}\hat{k}_\perp^2 >> \hat{\sigma}^{-1}$. This does not mean that the loop voltage to sustain the toroidal plasma current is influenced by the current diffusivity. The current diffusion is effective for microscopic structures. When the relation $\hat{\lambda} << \hat{\sigma}^{-1}$ holds, the loop voltage is not affected by the anomalous transport. These conditions for the magnetic Reynolds number $\hat{\sigma}$ are combined as

$$(c/a\omega_p)^2\alpha^{1/2} >> \hat{\sigma}^{-1} >> (c/a\omega_p)^4\alpha^{3/2}, \tag{53}$$

where we use the relations $\hat{\lambda} \sim (c/a\omega_p)^4\alpha^{3/2}$ and $\hat{k}_\perp \sim (a\omega_p/c)\alpha^{-1/2}$. Equation (53) is usually satisfied for present day experiments. When the temperature becomes low, the condition $\hat{\lambda}\hat{k}_\perp^2 >> \hat{\sigma}^{-1}$ may not be satisfied. This case is discussed later in relation to the pseudo classical confinement.

5.3 Characteristics of Fluctuations

The least stable mode gives the typical wave number for the self-sustained turbulence. Substituting Eq.(51) into Eq.(49-2), the characteristic mode number is given as

$$k_\perp = \frac{u(s)}{\sqrt{\alpha}} \frac{\omega_p}{c} \tag{54}$$

where the numerical coefficient u(s) is close to unity in the low shear limit and is about 0.1 for the parameter of s≈1 [8,15]. This result shows that the characteristic scale length is given by the collisionless skin depth, and that the scale length becomes longer as the pressure gradient increases. The fluctuation level is also given as

$$\frac{e\tilde{\varphi}}{T} \simeq \frac{eB}{T}\chi = \frac{q^2}{f(s,\alpha)}(-R\beta')^{3/2}\left(\frac{c}{\omega_p}\right)^2 \frac{v_A}{R}\frac{eB}{T} \tag{55}$$

showing that the fluctuation level is enhanced as the pressure gradient is increased, $e\tilde{\varphi}/T \propto \alpha^{3/2}$. The dependence on the pressure gradient is the same as the case of CDIM turbulence: the difference appears in the geometrical factors.

5.4 Connection to the Pseudo-Classical Transport and Bohm-Diffusion

This frame work of the self-sustained turbulence is applied to the low temperature plasma, and the connection between the L-mode and Pseudo-classical transport can be explained [29]. When the plasma temperature is low, the driving source of the mode is

Ξ rather than Λ in the nonlinear dispersion relation (45). The generalized form of nonlinear marginal equation is given, instead of Eq.(48), as

$$\frac{\alpha}{\hat{\sigma}\hat{\chi}} = \frac{c_1(1+c_2\rho N^2)}{(1+\rho N^2)^2(1-N^4)^2}\left(1+\frac{2s^2}{c_1}\frac{1+\rho N^2}{1+c_2N^2}N^4\right) \tag{56}$$

where ρ is the ratio $\rho = \hat{\sigma}\hat{\lambda}\sqrt{\frac{\alpha}{\hat{\chi}\hat{\mu}}}$ and coefficients are defined as $c_1 = 1/2+\alpha-s+s^2$, $c_2 = (1/2+\alpha-s)/c_1$.

Equation (56) determines the least stable mode and transport coefficient, as is shown in Fig.9. In the high temperature limit, $\rho\to\infty$, Eq.(56) reduces to Eq.(48). If the temperature is low and the relation

$$\hat{\sigma} < \hat{\chi}^{-1/3}(a\omega_p/c)^{4/3} \tag{57}$$

holds, the resistivity, rather than the current diffusivity, determines the growth of the mode. The analysis on the resistive ballooning mode [30] is recovered. In such a case, the transport coefficient is given as $\hat{\gamma} = 2\alpha/\hat{\sigma}$, or in a dimensional form as

$$\chi = \left(\frac{4\varepsilon r}{L_p}\right)\nu_{ei}\,\rho_{pe}^2 \tag{58}$$

where L_p is the pressure gradient scale length, β/β', ν_{ei} is the electron ion collision frequency and ρ_{pe} is the electron poloidal gyro radius. This formula is very close to the one obtained by Yoshikawa for the Pseudo-classical transport [31]. The change from Pseudo-classical confinement to L-mode confinement takes place at the condition Eq.(57). [This result is compared to the experiments in the spherator [31], where the transition between Pseudo-classical transport to the neo-Bohm transport was found to occur around T=10eV. For the parameters of experiments, the transition between the pseudo classical transport and L-mode confinement is predicted to occur at T=8eV from Eq.(57).]

Although various mechanisms could give rise to the Bohm diffusion [4], the connection with Bohm diffusion can also be discussed along this line of thought. The relation between the fluctuation level and the diffusivity gives the upper bound of the anomalous transport. The upper bound of fluctuation level, $|\tilde{n}/n| \leq 1$, or $|e\tilde{\phi}/T| \leq 1$, gives the upper bound of χ, from Eq.(38), as

$$\chi \simeq \mu \leq \frac{T_e}{eB} \tag{59}$$

except a numerical coefficient of the order unity.

These results Eqs.(52), (58), (59) show that the confinement characteristics changes from L-mode to Bohm confinement via Pseudo-classical confinement. The historical development of the confinement in Fig.10 seems to be understood from the consideration of the self-sustained turbulence.

6. Electric Field Bifurcation and Physics of the H-mode

The H-mode is characterized by the abrupt and spontaneous formation of the steep edge pressure gradient, often associated with the repetitive bursts of plasma across the surface [32]. In order to understand the formation of this steep transport structure, we have proposed the mechanism of the radial electric field bifurcation [33]. The radial electric field structure has multifold solutions, transition between which occurs at a critical pressure gradient. The strong electric field that is localized near the edge has a nature to suppress the cross-field transport, so as to strengthen the edge pressure gradient [34]. This theoretical picture, at this moment, is supported by experimental observations [35].

6.1 Generation and Bifurcation of the of Radial Electric Field

The radial electric field is generated by the radial current. Poisson's equation can be written as $\varepsilon_0\varepsilon_\perp \frac{\partial}{\partial t} E_r = e(\Gamma_e - \Gamma_i)$ where $\varepsilon_\perp$ is the perpendicular dielectric

constant, and Γ_e and Γ_i are the radial fluxes of electrons and ions, respectively. The stationary state equation,

$$\Gamma_e[X, X'; \nabla p \cdots] = \Gamma_i[X, X'; \nabla p \cdots], \qquad (60)$$

determines the structures of the radial electric field as a function of the plasma profiles, $X(r\,;\, \nabla p \cdots)$ (X being the normalized radial electric field, $X \equiv e\rho_p E_r / T_i$ and ρ_p is the poloidal ion gyroradius)

Equation (60) predicts the bifurcation of the solution X (X' and X", as well). Since plasma transport coefficients are dependent on the electric field structure, this bifurcation in the radial electric field causes those in the plasma transport. Theories of the H-mode are classified into two, depending on the relation between the gradient and flux. Figure 11 illustrates, for the two cases, the relation between the fluxes, radial electric field and fluctuation level, as a function of the gradients ∇n and ∇T. Figure 11(a) shows a *hard transition* model. In this case, the flux (and fluctuation level etc.) takes multiple values at certain values of the fixed gradients. Figure 11(b) presents those for a *soft-transition* model, where the flux can be a decreasing function of the gradients, but is single-valued. If the system has a hard transition, a soft transition is also available by the change of parameters. The cusp-type bifurcation (for the case of a hard transition) is obtained [36] as is illustrated in Fig.11(c). The change from the low to the high confinement state ("A" to "B" in Fig.11(c)) could occur either by crossing the transition points, or by following a smooth change. The Itoh-Itoh model and Shaing model belong to the case of a hard transition [33,37]. Those in [38] belong to the class of a soft transition.

There are many processes which are associated with the radial current [3]. Poisson equation is explicitly written, for singly charged ions, as

$$\frac{\varepsilon_0 \varepsilon_\perp}{e} \frac{\partial}{\partial t} E_r = \Gamma_{e-i}^{anom} - \Gamma_i^{lc} - \Gamma_i^{bv} - \Gamma_i^{v\nabla v} - \Gamma_i^{NC} + \Gamma_e^{NC} - \Gamma_i^{cx} \quad . \qquad (61)$$

The terms on the right hand side represent the following processes. (i) Γ_{e-i}^{anom} ; the bipolar part of the anomalous cross field flux (i.e., the excess flux of electrons relative to ions), (ii) Γ_i^{lc} ; the loss cone loss of ions, (iii) Γ_i^{bv} ; the bulk viscosity coupled to the magnetic field inhomogeneity, (iv) $\Gamma_i^{v\nabla v}$; the Reynolds stress in the global flow, (v) Γ_i^{NC} and Γ_e^{NC} ; the collisional flux (e.g., the ripple diffusion, or the contribution of the gyro-viscosity), (vi) Γ_i^{cx} ; the ion loss owing to charge exchange. The external-driven rf-waves can contribute to the term of Γ_{e-i}^{anom}. In order to provide a perspective, we choose some of the characteristic terms. Qualitative dependencies of these terms are shown as $\Gamma_{e-i}^{anom} \sim \hat{D}[X,X'](\lambda_p - X) + \hat{\mu}_\perp[X,X']\hat{\nabla}_\perp^2 X$, $\Gamma_i^{lc} \sim f_{lc}\nu_i\rho_p n_i \exp(-X^2)$, $\Gamma_i^{bv} = \frac{\varepsilon^2 n_i T_i}{erB}(X + X_0)\,\mathrm{Im}\, Z(X + i\nu_{**})$, where $\lambda_p = -\rho_p(\nabla n/n + \alpha_0 \nabla T/T)$ is the normalized gradient, $Z(X + i\nu_{**})$ is the plasma dispersion function, $X_0 = -\rho_p(n'/n + \gamma_{NC}T_i'/T_i) + V_{ill}/v_{thi}$, and $\nu_{**} = \nu_i qR/v_{thi}$. The numerical coefficient f_{lc} is a function of geometrical factors such as ε. The formula of Γ_i^{bv} is given in [39]. In the more collisional case, we have $\Gamma_i^{bv} \sim \varepsilon^2\nu_i\rho_p n_i \frac{X + X_0}{\nu_{**}^2 + X^2}$.

A first example of bifurcation is given by the balance between Γ_{e-i}^{anom} and Γ_i^{lc} [33] and another is obtained by that between Γ_i^{lc} and Γ_i^{bv} [37]. Figure 12 illustrates these examples of bifurcation. It is seen from this figure that the radial electric field shows a hard transition at critical plasma parameters.

6.2 Suppression of Turbulence

In the case of the H-mode, the inhomogeneity of the radial electric field plays the role in suppressing the turbulence [34]. We extend the method of self-sustained turbulence in the presence of the radial electric field inhomogeneity, in order to obtain the theoretical formula which describes both the L-mode and H-mode simultaneously.

The self-sustained turbulence is solved in an analytic manner for ballooning mode turbulence and interchange mode turbulence [40,41]. For simplicity, the one for the interchange mode turbulence is shown as [40]. The dc-component of the radial electric field, φ_0, is kept in Eqs.(10)-(12). The eigenmode equation for the dressed test mode is given as

$$\frac{d}{d\hat{k}}\frac{\hat{k}_\perp^2}{\hat{\gamma}+\hat{\lambda}\hat{k}_\perp^4}\frac{d}{d\hat{k}}\left(\hat{\gamma}+\hat{\chi}\hat{k}_\perp^2+\omega_{E1}\frac{d}{d\hat{k}}\right)\tilde{p}+\frac{q^2G_0}{s^2}\tilde{p}$$
$$-\frac{q^2}{\hat{k}_\theta^2 s^2}\left(\hat{\gamma}+\hat{\mu}\hat{k}_\perp^2+\omega_{E1}\frac{d}{d\hat{k}}\right)\hat{k}_\perp^2\left(\hat{\gamma}+\hat{\chi}\hat{k}_\perp^2+\omega_{E1}\frac{d}{d\hat{k}}\right)\tilde{p}=0 \qquad (62)$$

where

$$\omega_{E1}=\bar{k}_\theta\tau_{Ap}E_r'/B \qquad (63)$$

denotes the normalized shear flow velocity due to the inhomogeneous radial electric field. If one takes the limit of $\omega_{E1}\to 0$, Eq.(62) reduces to Eq.(18). The stationary state is obtained by use of the same procedure in section 3. Expanding the eigen function in terms of the Hermite functions, the effect of the electric field inhomogeneity is treated perturbatively. The transport coefficient is given as

$$\chi\sim\frac{1}{\left(1+0.5G_0^{-1}\omega_{E1}^2\right)}\frac{q^2G_0^{3/2}}{s^2}\left(\frac{c}{\omega_p}\right)^2\frac{v_{Ap}}{a} \qquad (64)$$

with the ion and electron viscosities of the same magnitude [40].

The typical level and correlation length of the fluctuations are dependent on the gradients of the pressure and electric field as

$$\langle k_\perp^2\rangle\propto\left(1+0.5G_0^{-1}\omega_{E1}^2\right)\frac{1}{G_0}\left(\frac{\omega_p}{c}\right)^2. \qquad (65)$$

$$\frac{e\tilde{\varphi}}{T}\sim\frac{1}{\left(1+0.5G_0^{-1}\omega_{E1}^2\right)}\frac{q^2G_0^{3/2}}{s^2}\left(\frac{c}{\omega_p}\right)^2\frac{v_{Ap}}{a}\frac{eB}{T}. \qquad (66)$$

These results show that the correlation length becomes shorter and the fluctuation level decreases owing to the electric field shear.

The same argument is extended to tokamak plasma transport based on current diffusive ballooning mode turbulence. The result is given as

$$\chi \sim \frac{1}{(1 + h_1\omega_{E1}^2 + h_2\omega_{E2}^2)} \frac{\alpha^{3/2}}{f(s,\alpha)} \left(\frac{c}{\omega_p}\right)^2 \frac{v_A}{qR} \qquad (67)$$

where numerical coefficients (h_1, h_2, f) are functions of s and α (see [41] for the details.) ω_{E2} denotes the curvature of the radial electric field. The ion viscosity also follows the formula Eq.(67). The characteristic scale length of the fluctuations is also shown to decrease by a similar factors if the electric field shear is increased.

The results Eqs.(64) and Eq.(67) indicate that the electric field inhomogeneity, as a whole, suppress the anomalous transport, so long as it is not too large. The efficiency for the suppression (the coefficient of the inhomogeneity parameters) depends on the pressure gradient and other plasma parameters. Both the gradient and curvature of the electric field is effective in reducing the transport coefficient.

6.3 Hysteresis , Limit Cycle and ELMs

A hard transition model can predict a fast transition at the critical points. This system has hysteresis and can generate a limit cycle oscillation. Figure 13 illustrates the loss rate as a function of a plasma parameter in the case of a hard transition type [42]. This curve belongs to the family of the *backward* bifurcation (which usually appears in sub-critical turbulence). There is hysteresis, as is shown by the dotted line. The central branch is thermodynamically unstable, so that a limit cycle oscillation is possible. This dynamics is discussed in relation to ELMs (Edge localized Modes) [43].

The transport equations of the plasma parameters and the electric field are given in a symbolic form by using the nonlinear transport coefficients as

$$\frac{\partial}{\partial t} n(r) = \nabla \cdot D[X, X'; n(r), T(r), \cdots] \nabla n(r) + S_p \qquad (68\text{-}1)$$

$$\frac{\partial}{\partial t} T(r) = \nabla \cdot \chi[X, X'; n(r), T(r), \cdots] \nabla T(r) + P \qquad (68\text{-}2)$$

$$\upsilon\frac{\partial}{\partial t}X(r) = \nabla\cdot\mu[X, X'; n(r), T(r),\cdots]\nabla X(r) + N[X, X'; n(r), T(r),\cdots] \quad (68\text{-}3)$$

where S_p is the particle source and P is the heating power. (In general, terms like 'pinch' can also be included in Eqs.(68-1) and (68-2).) The coefficient υ indicates the fact that the time scale in Eq.(61), determined by the flux and viscosity, may be much faster than the usual transport process for the temperature and density. The nonlinear term N in Eq.(68-3) indicates those source terms of the radial electric field in Eq.(61), which allow a bifurcation of the hard transition type. The transport coefficient is given in the form (e.g., Eq.(64) or (67)) $\mu = \mu[X, X'; n(r), T(r),\cdots]$. This set of equations belongs to the type of the extended-time-dependent Ginzburg-Landau equation (E-TDGL equation).

The system of dynamical equations of the E-TDGL type, Eq.(68), predicts a limit cycle oscillation, which is the sequence of the transitions and back transitions [42,44,45]. In this analysis, the parameter g that controls the transport was chosen as $g \equiv \frac{\rho_p}{L_n}\frac{\hat{D}_L}{\nu_i\rho_p^2}$ and N is modelled by a quadratic equation of X. Figure 14 illustrates the limit cycle oscillation seen in the flux out of the plasma with the radial profile of the transport coefficient. The H-phase and L-phase are realized one by one. In the H-phase, the confinement is good so that an increment in the parameter occurs. Owing to this improvement, e.g., the density becomes too high, so that the condition g_m in Fig.13 is reached. Then a sudden increment in the loss rate takes place, causing a jump of the out flux and a rapid decay of the pedestal profile. If the plasma parameter changes and the parameter g increases, the condition g_M in Fig.13 is realized. Then the transition to the H-phase takes place. These processes repeat themselves. Under a constant supply of plasma from core, a limit cycle oscillation occurs. This is the self-organized oscillation generated by the hysteresis and hard transition in the plasma transport and electric field generation. This limit cycle oscillation is possible near the threshold condition of the L-H transition, which is evaluated in the stationary state [42]. Small and frequent ELMs are observed experimentally in the vicinity of the threshold

power for the L-H transition, and are called dithering ELMs. This limit cycle oscillation constitutes a model of this kind of ELMs.

The appearance of this limit cycle oscillations is very abrupt when the global plasma parameter evolves slowly in time. As the plasma parameters reach the threshold condition, the first burst appears, followed by periodic bursts (see, e.g., [45]). Finally the self-regulated oscillation suddenly disappears and a stationary H-mode is established. The oscillation amplitude jumps abruptly from zero to finite value and from finite amplitude to zero. This feature is characteristic of the hard type of bifurcation which contains a hard-transition and hysteresis. The oscillations can also be found in the case of a soft bifurcation (normal bifurcation or pitch-fork bifurcation). The limit cycle oscillation can also be available in this type [46]. Like the Hopf bifurcation, the limit cycle appears gradually under the gradual change of the global parameter. This is one of the points that discriminate the models.

7. Application to Tokamak Transport Analysis

The form of χ in Eq.(52) is consistent in various aspect of the L-mode transport characteristics, i.e.,

- degradation of τ_E by intense heating,
- large χ near the edge,
- improvement of τ_E by the heavier isotope,
- dependence of τ_E on the plasma current,
- weak dependence of temperature on the magnetic field,
- weak dependence of temperature profile on the heating profile,
- larger χ^{HP} than χ,
- μ is enhanced to the level of χ,

and so on. Detailed comparison by use of the transport code has been performed [47], which is explained in the following.

7.1 Transport Equations

In the numerical simulation, we solve the one-dimensional transport equation. The transport code TASK/TR [48] is employed. We solve the development of plasma temperatures, T_e and T_i, and the poloidal magnetic field B_θ. In the present simulation, the density profile is fixed in time as $n_e(r) = (n_e(0) - n_s)(1 - (r/a)^{m_1})^{m_2} + n_s$. The one-dimensional transport equations are given as

$$n\frac{\partial}{\partial t}T_e - \frac{1}{r}\frac{\partial}{\partial r}rn\chi_e\frac{\partial}{\partial r}T_e = P_{He} + P_{OH} - P_{ei} - P_{rad} \tag{69-1}$$

$$n\frac{\partial}{\partial t}T_i - \frac{1}{r}\frac{d}{dr}rn\chi_i\frac{d}{dr}T_i = P_{Hi} + P_{ei} \tag{69-2}$$

$$\frac{\partial}{\partial t}B_\theta = \frac{\partial}{\partial r}\eta_{NC}\left(\frac{1}{r}\frac{\partial}{\partial r}rB_\theta - J_{BS} - J_{LH}\right) \tag{69-3}$$

In the energy balance equations (69-1) and (69-2), P_{OH} denotes the joule heating power, P_{ie} the equipartition power, P_{He} and P_{Hi} the additional heating power, respectively. The magnetic diffusion equation (69-3) includes the neoclassical resistivity η_{NC}, the Bootstrap current J_{BS} and the current driven by the Lower hybrid waves, J_{LH}. As is discussed by Eq.(53), the anomalous current diffusivity very little influences the evolution of the global current profile and is not kept in Eq.(69-3).

The Ohmic heating power is calculated by use of the neoclassical resistivity $P_{OH} = \eta_{NC} J (J - J_{BS} - J_{LH})$ where J is the plasma current. The neoclassical transport coefficients are used according to [49]. Power deposition profile of additional heating is assumed to be Gaussian and parameterized as $P_H(r) = \sum_j P_{H,j} \exp\left\{-(r - r_{H,j})^2 r_{w,j}^{-2}\right\}$. Here we take the $j = 0$ heating component and choose the parameters $r_{H,0} = 0$ and $r_{w,0} = a / 2$ for standard calculation. Bootstrap current is taken into account as the non-inductive current drive in this simulation. The Bootstrap current J_{BS} is calculated according to the neoclassical formula in [49]. The analysis for the case of LH current drive is given in [47,50].

The transport coefficients are given as a sum of the turbulent term χ_{TB} and the neoclassical term χ_{NC} as $\chi = \chi_{TB} + \chi_{NC}$. The electron and ion diffusivities are not

separated in the present turbulent transport model: we here assume that they have the same magnitude. Taking into account of the uncertainty of the order unity in the theoretical formula of χ_{TB}, in Eq.(52) we introduce a numerical factor C_{TB} in simulations. (Note that the one point renormalization underestimates the numerical coefficient [51].) The turbulent thermal diffusivities are given

$$\chi_{TB} = C_{TB} \frac{q^2}{f(s,\alpha)} (-R\beta')^{3/2} \left(\frac{c}{\omega_p}\right)^2 \frac{v_A}{R} \tag{70-1}$$

with the fitting formula for $f(s,\alpha)$ as

$$\frac{1}{f(s,\alpha)} = \frac{(1+\kappa)^{5/2}}{\sqrt{2(1-2s')[1-2s'+3s'^2(1+\kappa)]}} \tag{70-2}$$

where κ is the average good curvature and $s' = s - \alpha$. When the q value is below unity, the average magnetic curvature becomes a bad one, and the formula Eq.(36) is used. By choosing the numerical constant C_{TB} as $C_{TB} \simeq 12$, the energy confinement time in the L-mode regime and the improved confinement was simulated. (See [50] for the details of the simulations.)

7.2 L-mode Confinement

The plasma parameters are taken in the range of the large tokamaks. We choose, as standard parameters, a = 1.2m, R = 3m, B = 3T, and the central electron density $n_e(0) = 5\times 10^{19}m^{-3}$.

Figure 15 shows the stationary plasma profile in the OH heating and additional heating (20MW). In both cases, the thermal conductivity has the shape to increase near the plasma edge. This is mainly due to the profiles of the safety factor and density. The shapes of the electron temperature profile are similar to OH and additional heating cases, so as to recover the *profile resilience*.

Dependence of the energy confinement time on various parameters are studied. It is found, by the numerical simulation,

$$\tau_{E,th} \propto P_{tot}^{-0.6} B_t^0 n_e^{0.6} I_p^{0.8} \tag{71}$$

in the large current limit, where the suffix th indicates that only the thermal component is taken into account in evaluating the energy confinement time. This result is similar to the one obtained in the empirical scaling law [52], except the stronger density dependence obtained here. This is because the energetic component is included in the total energy confinement time; much stronger density dependence, $\tau_{E,th} \propto n_e^{0.5}$, was confirmed if one measures the thermal component [53].

The dependence on the plasma current is shown in Fig.16. At high current limit, the energy confinement time increases with I_p. It should be noted that, in the low current limit, the energy confinement time starts to increase and can be twice better than the L-mode plasmas. The mechanism of this improved confinement is related to the current profile modification, and is discussed in the next subsection.

7.3 Current Profile Control and Improved Confinement

The influence of the current profile is predicted based on the transport coefficient Eq.(70). The impacts of the low/negative magnetic shear and that of the change in the internal inductance ℓ_i are explained. This feature of the turbulent transport coefficient was attributed to the origin of the confinement improvement in the high-β_p mode [54], the PEP mode [55], and high-ℓ_i. confinement [56].

In a weak shear or the negative shear region, $s < 1/3 + \alpha$, the increment of χ associated with α becomes very gradual. For the fixed pressure gradient, χ shows a noticeable reduction if the magnetic shear enters in this domain, as is shown in Fig.8. The reduction of the thermal conductivity is expected, roughly speaking, in the domain of the second stability. Note that large Shafranov shift is also predicted to cause the reduction in transport.

This shear dependence gives rise to the formation of the internal transport barrier. Figure 17 illustrates the radial profile of the improved confinement mode in the low current limit, i.e., high-β_p plasmas. The internal transport barrier, associated with the low magnetic shear, is demonstrated. As the pressure gradient increases so as to reach the region

$$\beta_p \gtrsim 1 \tag{72}$$

the Bootstrap current is large enough to affect the total current profile. The Bootstrap current is driven in the middle of the plasma so as to make the plasma current flatter. The reduced shear makes the transport coefficient lower. If the thermal conductivity is reduced, the pressure gradient increases. The increment of the pressure gradient leads to the enhancement of the Bootstrap current, which causes more prominent flattening of the current. The stronger flattening further decreases the thermal conductivity, enhancing the pressure gradient further. Thus the internal transport barrier is self-organized. The energy confinement time for this high-β_p mode is fitted as

$$\tau_E \sim \beta_p^{0.76} \tau_E(\mathrm{L-mode}) \qquad \text{for } \beta_p \gtrsim 1 \tag{73}$$

This improved confinement is easy to occur if the heating power is localized near the plasma center [50]. The isotope effect becomes more prominent if coupled with the improvement of High-β_p mode. In the high-β_p mode, the isotope dependence of

$$\tau_E \propto A_i^{0.8} \tag{74}$$

was predicted [57].

The other way for improved confinement is predicted by peaking the current profile, if the current is large and the Bootstrap current is not effective. For fixed current, the higher internal inductance implies that the internal q-value is lower. Due to

the q-dependence in the thermal conductivity, the higher internal inductance enhances the total energy confinement. The internal inductance is varied by the rapid current ramping. The numerical simulation yields the dependence

$$\tau_E \propto \ell_i^{-0.6}. \tag{75}$$

The current profile modification thus has the potential to improve the energy confinement time. Applications by use of the Lower hybrid current drive, NBI current drive, current ramp-up/down have also been studied based on this transport modelling. See [47,50] for detailed analysis and comparison with experiments.

8. Summary

In this article, we overviewed our recent studies on the theory of turbulent transport. The concept of the self-sustained turbulence is extended. The plasma turbulence has the nature of subcritical turbulence: the anomalous transport further destabilizes the fluctuations through the scattering of electrons. The stationary state is realized by the balance between the nonlinear destabilization and nonlinear stabilization. Combining the plasma dynamics and that of electromagnetic field, the transition in transport was predicted to occur. The hysteresis is generated by the electric field bifurcation, causing the transition as well as limit cycle oscillations.

In the turbulent transport, the parameter "*gradient*" is taken into as the *order parameter*. The transport coefficient is increased, the correlation length becomes longer and the fluctuation level gets higher as the pressure gradient increases. These features are the characteristics of the transport processes in non-equilibrium matter. It is in contrast to the collisional diffusion, which is generated by the thermal fluctuations, i.e., Coulomb collision. The dynamics behaviour of the nonlinear fluctuations has also been studied in the framework of the self-sustained turbulence. The analysis is reported in [58].

The normalized plasma gradient is summarized as

$$\Im = \left(\frac{q}{s}\right)^{4/3} G_0 \frac{(\lambda_N + \lambda_c)^{2/3}}{(\chi_N + \chi_c)(\mu_N + \mu_c)^{1/3}} \quad \text{(CDIM turbulence)} \qquad (75)$$

which we tentatively called Itoh number after Rayleigh number in the Bernard cell convection problem $\Re_a = \frac{Agd^4 \nabla T}{\nu_c \chi_c}$ (d: distance of two plates, Ag: bouyancy by gravity). In plasmas, the nonlinear marginal stability condition is given as $\Im = \Im_c$, while that in Rayleigh-Benard problem is given as $\Re_a = \Re_{ac}$. In both cases, the gradient drives instability and the enhanced viscosity and conductivity suppress the instability. What is noticeable for plasmas is that the dissipation, through the current diffusivity (i.e., the electron viscosity), can *enhance* the driving force. This is one of the basic feature of the plasma turbulence, which is revealed by this theoretical approach. The division of the dissipated energy between electrons and ions was found to be nearly equal [59].

By the simulation study, it is demonstrated that the nonlinear destabilization of the perturbations takes place when the amplitude exceeds the threshold. The saturation level is enhanced by the convective nonlinearity, but is not sensitive to the linear growth rate itself. Comparing with the theory based on the renormalization of turbulence, the simulation confirms the picture of self-sustained turbulence. The estimation of χ_N using the mean field approximation is also confirmed within an uncertainty of the numerical factor.

The argument based on the scale invariance method has confirmed this result [60]. Connor has extended the model in the case that the electron pressure term is more important in the Ohm's law than the parallel electric field. In such a case, Eq.(51) has additional coefficient by the factor of $(v_e/v_A\sqrt{\alpha})$ [60]. This change in the factor stimulates the future extension of this methodology to more general basic equations.

One of the main extension is to include the effect of the magnetic braiding [60,61]. Analysis for the onset of the fast nonlinear growth was developed to study the magnetic trigger problem in sawtooth physics [62]. It was shown that at certain pressure gradient, which is occasionally not far from the linear ideal MHD instability boundary,

the self-sustained magnetic braiding sets in and the transport coefficient is subject to new transition to higher level [61,63]. This process provides the picture for the giant ELMs [63] or crash of the pressure [64].

These results on transport coefficients and fluctuations supply the explanation for experimental observations, and some of the applications is reported in section 7. Simultaneous explanations for various confinement-mode (e.g., L-mode transport, internal transport barrier and H-mode) are searched for, starting from one set of basic equations. At the same time, more mysterious nature of confined plasmas is recognized and waits novel theories; e.g., a rapid response in the transport [65,66], or the flows against the gradients [67]. Including the formulation of the transport matrix or the method of TSDIA (two-scale direct interaction approximation) [68], the efforts leading to the new break-through in confinement theory are still required.

Acknowledgements

Authors wish to acknowledge Acad. V. D. Shafranov for inviting them to prepare the article for the memorial volume of Prof. V. I. Petviasivili. They also cordially thank Dr. M. Azumi, Dr. J. W. Connor, Prof. A. J. Lichtenberg, Dr. H. Sanuki , Prof. F. Wagner for various discussion on the problem. This work is partly supported by the Grant-in-Aid for Scientific research of Ministry of Education Japan and by the collaboration programme of Advanced Fusion Research Center of Kyushu University.

References

[1] B. B. Kadomtsev and V. I. Petviasivili: *Soviet Physics-Doklady* **15** (1970) 539.

[2] V. I. Petviasivili: *Soviet Physiscs-Tech. Phys.* **12** (1967) 144.

[3] K. Itoh and S.-I. Itoh *Plasma Phys. Cont. Fusion* **38** (1996) 1.

[4] B. B. Kadomtsev : *Plasma Turbulence* (Academic Press, 1965, New York).

[5] A. B. Mikhailovskii : *Electromagnetic instabilities in an inhomogeneous plasma* (IOP Publishing, 1992, Bristol).

[6] For recent comparison study, see, e.g.,
J. W. Connor, G. P. Maddison, H. R. Wilson, G Corrigan, T. E. Stringer and F. Tibone: *Plasma Phys. Contr. Fusion* **35** (1993) 319.

[7] S. P. Hirshman and K. Molvig: *Phys. Rev. Lett.* **42** (1979) 648.
D. Biskamp and M. Walter: Phys. Lett. **109A** 34 (1985).
R. D. Sydora, J. N. Leboeuf, T. Tajima: *Phys. Fluids* **28** (1985) 528.
M. Wakatani and A. Hasegawa: *Phys. Rev. Lett.* **59** (1987) 1581.
B. D. Scott *Phys. Fluids B* **4** (1992) 2468.
B. A. Carreras, V. E. Lynch, L. Garcia, P. H. Diamond: *Phys. Fluids B* **5** (1993) 1491.

[8] K. Itoh, S.-I. Itoh and A. Fukuyama: *Phys. Rev. Lett.* **69** (1992) 1050.
K. Itoh, S.-I. Itoh, A. Fukuyama, M. Yagi, M. Azumi : *Plasma Phys. Cont. Fusion* **36** (1994) 279.

[9] V. D. Shafranov, E. I. Yurchenko: *Sov. Phys. JETP* **26** (1968) 682.

[10] C. Gouldon, D. Marty, E. K. Maschke, J. P. Dumon: *Plasma Physics and Controlled Nuclear Fusion Reserach* (IAEA, Vienna, 1968) Vol.1, 847.
A. Mohri: *J. Phys. Soc. Jpn.* **28** (1970) 1549.
K. Uo: *Plasma Phys.* **13** (1971) 243.

[11] B. B. Kadomtsev, O. P. Pogutse: *Sov. Phys. JETP* **38** (1974) 283 [ZhETF **65** (1973) 575].

H. R. Strauss: *Phys. Fluids* **20** (1977) 1354.

[12] R. D. Hazeltine: Phys. Fluids **26** (1983) 3242.

M. Yagi : Ph.D.. Thesis, Kyoto University (1989).

[13] K. Itoh, S.-I. Itoh, A. Fukuyama, M. Yagi, M. Azumi : *Plasma Phys. Cont. Fusion* **36** (1994) 1501.

[14] M. N. Rosenbluth and C. L. Longmire C L: *Ann Phys* (NY) **1** (1957) 120.

[15] M. Yagi, K. Itoh, S.-I., Itoh, A. Fukuyama, M. Azumi: *Phys. Fluids B* **5** (1993) 3702.

M. Yagi, K. Itoh, S.-I., Itoh, A. Fukuyama, M. Azumi: *J. Phys. Soc. Jpn.* **63** (1994) 10.

[16] K. Itoh, S.-I. Itoh, A. Fukuyama, M. Yagi, M. Azumi : *J. Phys. Soc. Jpn.* **62** (1993) 4269.

[17] R. L. Miller: *Private communications* (1992).

[18] T. Ohkawa: *Phys. Lett.* **67A** (1978) 35.

[19] V. V. Parail, O. P. Pogutse: *JETP Letters* **32** (1980) 384.

B. B. Kadomtsev, O. P. Pogutse: in *Plasma Physics and Controlled Nuclear Fusion Research 1984* (IAEA, 1985, Vienna) Vol.2, p.69.

[20] Yu. V. Gott, E. I. Yurchenko: *Plasma Physics Reports* **20** (1994) 769.

[21] L. S. Solov'ev and V. D. Shafranov: in *Reviews of Plasma Physics* (ed. M A Leontovich) Vol.5, p1 (Consultants Bureau, 1970, New York)

[22] S. Sudo, Y. Takeiri , H. Zushi, F. Sano, K. Itoh, K. Kondo, A. Iiyoshi: *Nucl. Fusion* **30** (1990) 11,

F. Sano, Y. Takeiri , K. Hanatani, H. Zushi, M. Sato, S. Sudo, T. Mutoh, K. Kondo et al : *Nucl. Fusion* **30** (1990) 81.

[23] K. Ida , H. Yamada, H. Iguchi, K. Itoh, CHS Group: *Phys. Rev. Lett.* **67** (1992) 58.

[24] H. Zushi , T. Mizuuchi , O. Motojima, M. Wakatani, F. Sano, M. Sato , A. Iiyoshi, K. Uo: *Nucl. Fusion* **28** (1988) 433.

[25] M. Yagi, S.-I. Itoh, K. Itoh, A. Fukuyama, M. Azumi: *Phys. Plasmas* **2** (1995) 4140.

[26] M. Yagi: *J. Plasma and Fusion Research* **71** (1995) 1123.

[27] A. Hasegawa, K. Mima: *Phys. Fluids* **21** (1978) 87.

See, for simulation study, e.g.,

M. Wakatani, K. Watanabe, H. Sugama, A. Hasegawa: *Phys. Fluids B* **4** (1992) 1754.

[28] J. W. Connor, R. J. Hastie, J. B. Taylor: *Proc. R. Soc. London A* **365** (1979) 1.

[29] K. Itoh, S.-I. Itoh, A. Fukuyama, M. Yagi, M. Azumi : *Phys. Fluids B* **5** (1993) 3299.

[30] B. A. Carreras, P. H. Diamond, et al. : *Phys. Rev. Lett.* **50** 503 (1983).

[31] S. Yoshikawa: *Phys. Rev. Lett.* **25** (1970) 353.

B. B. Kadomtsev in *Proc. 6th European Conf. Controlled Fusion and Plasma Physics*, Moskow 1973 (European Physical Society, Petit-Lancy, 1973) Vol.II, p.1.

S. Yoshikawa: Nucl. Fusion 13 (1973) 433.

[32] F. Wagner *et al* : *Phys. Rev. Lett.* **49** (1982) 1408.

ASDEX Team: *Nucl Fusion* **29** (1989) 1959.

[33] S.-I. Itoh and K. Itoh: *Phys. Rev. Lett.* **60** (1988) 2276.

[34] S.-I. Itoh, K. Itoh, T. Ohkawa, N. Ueda: in *Plasma Physics and Controlled Nuclear Fusion Research 1988* (IAEA, 1989, Vienna) Vol.2, p23.

K. C. Shaing *et al*: n *Plasma Physics and Controlled Nuclear Fusion Research 1988* (IAEA, 1989, Vienna) Vol.2, p13.

H. Biglari, P. H. Diamond, P. W. Terry : *Phys. Fluids B* **2** (1990) 1.

[35] R. J. Groebner, K. H. Burrell, A. Seraydarian : *Phys. Rev. Lett.* **64** (1990) 3015.

K. Ida, S. Hidekuma , Y. Miura, T. Fujita, M. Mori, K. Hoshino, N. Suzuki, T. Yamauchi, JFT-2M Group:*Phys. Rev. Lett.* **65** (1990) 1364.

[36] S.-I. Itoh and K. Itoh: *Nucl. Fusion* **29** (1989) 1031.

[37] K. C. Shaing, E. Crume Jr.: *Phys. Rev. Lett.* **63** (1989) 2369.

[38] T. Ohkawa, F. L. Hinton, C. S. Liu, Y. C. Lee: *Phys. Rev. Lett.* **51** (1983) 2102.

F. L. Hinton: *Phys. Fluids B* **3** (1991) 696.

V. Rozhanskii , M. Tendler:*Phys. Fluids B* **4** (1992) 1877.

P. H. Diamond, Y.-M. Liang, B. A. Carreras, P. W. Terry : *Phys. Rev. Lett.* **72** (1994) 2565.

H. Sugama, C. W. Horton: *Plasma Phys. Contr. Fusion* **37** (1995) 345.

[39] T. E. Stringer : *Nucl. Fusion* **33** (1993) 1249.

[40] K. Itoh, S.-I. Itoh, A. Fukuyama, H. Sanuki, M. Yagi : *Plasma Phys. Contr. Fusion* **36** (1994) 123.

[41] S.-I. Itoh, K. Itoh, A. Fukuyama, M. Yagi: Phys. Rev. Lett. **72** (1994) 1200.

[42] S.-I. Itoh, K. Itoh, A. Fukuyama, Y. Miura et al.: *Phys. Rev. Lett.* **67** (1991) 2485.

[43] M. Keilhacker *et al* : *Plasma Phys. Contr. Fusion* **26** (1984) 49.

P. Gohil *et al* :*Phys. Rev. Lett.* **61** (1988) 1603.

T. Ozeki*et al* : *Nucl. Fusion* **30** (1990) 1425.

[44] S.-I. Itoh, K. Itoh, A. Fukuyama: *Nucl. Fusion* **33** (1993) 1445.

[45] H. Zohm: *Phys. Rev. Lett.* **72** (1994) 222.

[46] See, e.g., P. H. Diamond, et al., *International Conf. Plasma Physics and Controlled Nuclear Fusion Research* (IAEA, Seville, 1994) paper D-2-II-6.

[47] A. Fukuyama et al: *Plasma Phys. Contr. Fusion* **36** (1994) 1385.

[48] T. Morishita, A. Fukuyama, Y. Furutani: *J. Phys. Soc. Jpn.* **57** (1988) 1238.

[49] F. L. Hinton and R. D. Hazeltine: *Rev. Mod. Phys.* **48** (1976) 239.

[50] A. Fukuyama, K. Itoh, S.-I. Itoh, M. Yagi, M. Azumi: *Plasma Phys. Contr. Fusion* **37** (1995) 611.

A. Fukuyama, K. Itoh, S.-I. Itoh, M. Yagi, M. Azumi:*Nucl. Fusion* **35** (1995) No.12, in press.

[51] P. H. Diamond and B. A. Carrearas: *Comments Plasma Phys. Contr. Fusion* **10** (1987) 271.

[52] P. N. Yushmanov, et al.: *Nucl. Fusion* **30** (1990) 1999.

[53] T. Takizuka et al.: *Proc. 19th European Conf. on Controlled Fusion and Plasma Heating* (Innsbruck, 1992) Vol.16C, part II, p51.
U. Stroth, M. Kaiser, F. Ryter, F. Wagner: *Nucl. Fusion* **35** (1995) 131.

[54] Y. Koide, et al: *Phys. Rev. Lett.* **72** (1994) 366.

[55] M. Keilhacker and JET Team: *Plasma Phys. Contr. Fusion* **33** (1991) 1453.

[56] M. Zahnstorff, et al.: *Plamsa Physics and Controlled Nuclear Fusion Research 1990* (Vienna, 1991, IAEA) Vol.1, p.109.

[57] A. Fukuyama, K. Itoh, S.-I. Itoh, M. Yagi, M. Azumi: *Comments Plasma Phys. Contr. Fusion* **15** (994) 309.

[58] K. Itoh, S.-I. Itoh, M. Yagi A. Fukuyama: *'Dynamic structure in self-sustained turbulence'* (Research Report NIFS-360, 1995) submitted to *Plasma Phys. Contr. Fusion.*

[59] S.-I. Itoh, K. Itoh, A. Fukuyama, M. Yagi, M. Azumi, K. Nishikawa: *Phys. Plasmas* **1** (1994) 1154.

[60] J. W. Connor: *Plasma Phys. Contr. Fusion* **35** (1993) 757.

[61] K. Itoh, S.-I. Itoh, A. Fukuyama, M. Yagi: *Plasma Phys. Contr. Fusion* **37** (1995) 707.

[62] A. J. Lichtenberg,.K. Itoh, S.-I. Itoh, A. Fukuyama: *Nucl. Fusion* **32** (1992) 495.

[63] S.-I. Itoh, K. Itoh, A. Fukuyama, M. Yagi : *'Edge localized modes as new bifurcation in tokamaks' Phys. Rev. Lett.* **76** (1996) in press.

[64] K. Itoh, S.-I. Itoh, A. Fukuyama: *Plasma Phys. Contr. Fusion* **37** (1995) 1287.

[65] E. D. Frederickson, K. McGuire, A. Cavallo, R. Budny, A. Janos, D. Monticello *et al*: *Phys. Rev. Lett.* **65** (1990) 2869.

M. Sakamoto, K. N. Sato, Y. Ogawa, K. Kawahata, S. Hirokura *et al*: *Plasma Phys. Contr. Fusion* **33** (1991) 583.

J. G. Cordey, D. G. Muir, S. V. Neudatchin, V. V. Parail, S. Ali-Arshad*et al*: *Plasma Phys. Contr. Fusion* **36** (1994) A267.

For further review, see, N. J. Lopes Cardozo: *Plasma Phys. Contr. Fusion* **37** (1995) 799.

[66] B. B. Kadomstev, K. Itoh, S.-I. Itoh: *Comments Plasma Phys. Contr. Fusion* **16** (995) 335.

P. H. Diamond, T. S. Hahm: *Phys. Plasmas* **2** (1995) 3640.

[67] T. C. Luce, C. C. Petty, J. C. M. deHaas: *Phys. Rev. Lett.* **68** (1992) 52.

K. Ida, Y. Miura, T. Matsuda, K. Itoh, S. Hidekuma, S.-I. Itoh, JFT-2M Group 1995 *Phys. Rev. Lett.* **74** 1990.

K. Nagashima, Y. Koide, H.Shirai: *Nucl. Fusion* **34** (1994) 449.

[68] A. Yoshizawa: *Phys. Fluids* **28** (1985) 1377.

Figure captions

Fig. 1 Schematic drawing of the growth rate as a function of back-ground fluctuation level. Solid line indicates the case of self-sustained turbulence, and dahed line is for the conventional picture.

Fig. 2 Eigenvalue H as a function of the mode number (a) and the learst stable mode determines the transport coefficient $h = \chi / \left[q^2 s^{-2} G_0^{3/2} (\lambda/\chi)\sqrt{\chi/\mu_\perp}\right]$ (b).

Fig. 3 The radial profile of the thermal diffusivity for the case of Heliotron-E plasma. Profiles are chosen such that $p_0(\hat{r}) = p_0(0)\left[1 - \hat{r}^2 + \Delta\right]$, $T(\hat{r})/T(0) = n(\hat{r})/n(0)$, $\Delta = 0.05$, $T(0) = 500$ eV, $B = 2T$, $n(0) = 5\times10^{19}$ m^{-3}, and $a/R = 0.1$. The hatched region indicates the experimental observation. The dotted line shows theoretical result, employing a multitplication factor 9.

Fig. 4 The maximum linear growth rate as a function of the pressure gradient G_0. (Parameters are: $\mu_c = \chi_c = 0.2$, $\lambda_c = 0.01$ and $s = 0.5$.)

Fig. 5 Fluctuating electric field energy versus time, showing the nonlinear growth due to the electron nonlinearlity at $t > 35$ (solid line). Parameters are $\mu_c = \chi_c = 0.2$, $\lambda_c = 0.01$ and $s = G_0 = 0.5$. The dahsed line indicates the simulation, for which the convective nonlinearity $[\phi, j]$ in the Ohm's law is omitted. (Quoted from [25].)

Fig. 6 Evolution of fluctuating pressure energy. (a)$\lambda_c = 0.01$ and (b) $\lambda_c = 0.01$ with linear Ohm's law and (c) $\lambda_c = 0.2$. The case (c) has a larger linear growth rate than the case (a). But the saturation level is less affected by the linear growth rate in (a) and (c). Other parameters are the same as in Fig.5. (Quoted from [25].)

Fig. 7 Nonlinear stability boundary in $\langle W_\phi \rangle - G_0$ plane. Parameters are the same as in Fig.5. The regions (1) and (2) represent the nonlinearly unstable regions with $\gamma_L > 0$, $\gamma_N \neq 0$, and $\gamma_L < 0$, $\gamma_N \neq 0$, respectively. The region (3) represents the linearly unstable region. (Quoted from [25].)

Fig. 8 Form factor $1/f(s,\alpha)$ as a function of s in the small-α limit. In the high shear region, the factor 1/f decreases as s increases. When the shear is very weak or negative, the coefficient 1/f becomes very small. The reflects the second stability against the ballooning mode.

Fig. 9 Marginal stability condition for the nonlinear ballooning mode instability (schematic). N stands for the normalized mode number. The resistive limit ($\rho \to 0$, (a)) and current diffusive limit ($\rho >> 1$, (b)) are shown.

Fig. 10 Historical evolution of confinement time.

Fig. 11 Relation between gradient and flux. Hard transition model (a) and soft transition model (b). The cusp-type bifurcation with hard transition is summarized in (c).

Fig. 12 Examples of the electric field bifurcation. In (a), the balance between $\Gamma_{e\text{-}i}^{anom}$ and the loss cone loss is shown. The self-consistent flux, as a function of the gradient, is shown in (b). In (c) another example, i.e., the balance between the loss cone loss (solid line) and Γ^{bv} (dashed line), is demonstrated. (Quoted from [33] and [37].)

Fig. 13 Schematic relation between the plasma parameter (g) and the diffusivity (i.e., the flux divided by the gradient). The dotted line indicate the hysteresis and the limit cycles.

Fig. 14 Periodic formation and destruction of the edge transport barrier give rise to the periodic bursts of the outflow. Note that the supply from the core is constant in time. (Quoted from [42].)

Fig. 15 Radial profile of the ion temperature and the ion thermal diffusivity. Cases of Ohmic heating and additional heating are shown. Parameters are a = 1m, R = 3m, B = 3T, I_p = 3MA, $n_e(0) = 5 \times 10^{19} m^{-3}$ for the deuterium plasma. (Quoted from [50].)

Fig. 16 Dependence of the energy confinement time on the plasma current. Heating power is taken as P = 10MW and other parameters are the same as in Fig.15. The broken curve indicates the ITER-89P L-mode scaling. In the low current limit, the enhancement over the L-mode scaling is found. (Quoted from [50].)

Fig.17 Radial profile with internal transport barrier. I_p =1MA, P = 20 MW and other parameters are the same as in Fig.15. (Quoted from [50].)

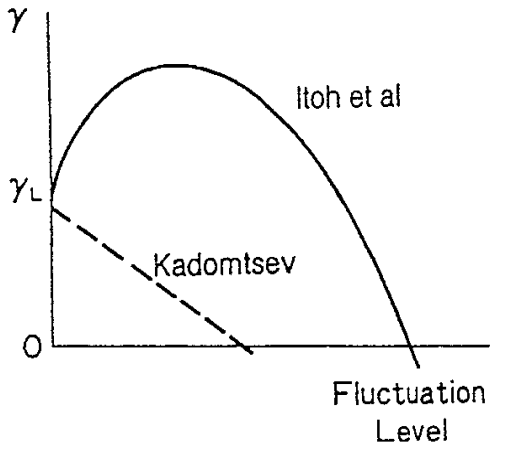
γ
Itoh et al
γL
Kadomtsev
0
Fluctuation
Level

Fig. 1

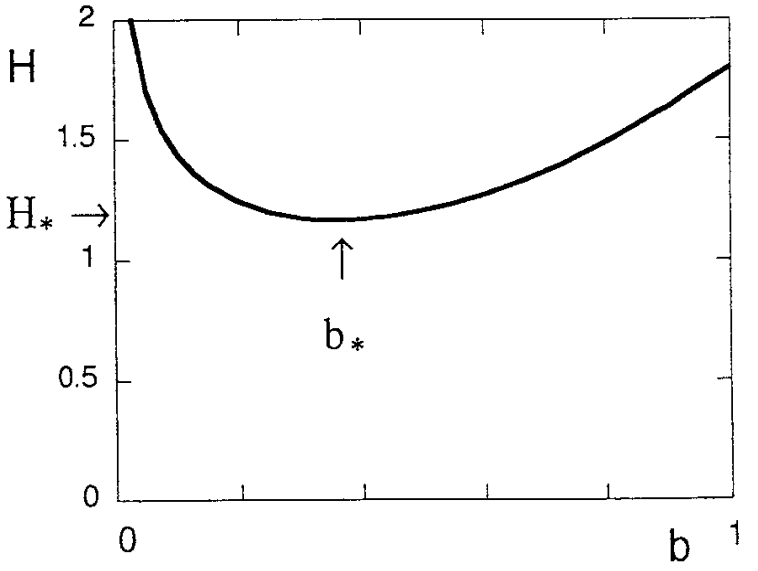
H
2
1.5
H* →
1
0.5
0
b*
0
b
1

(a)

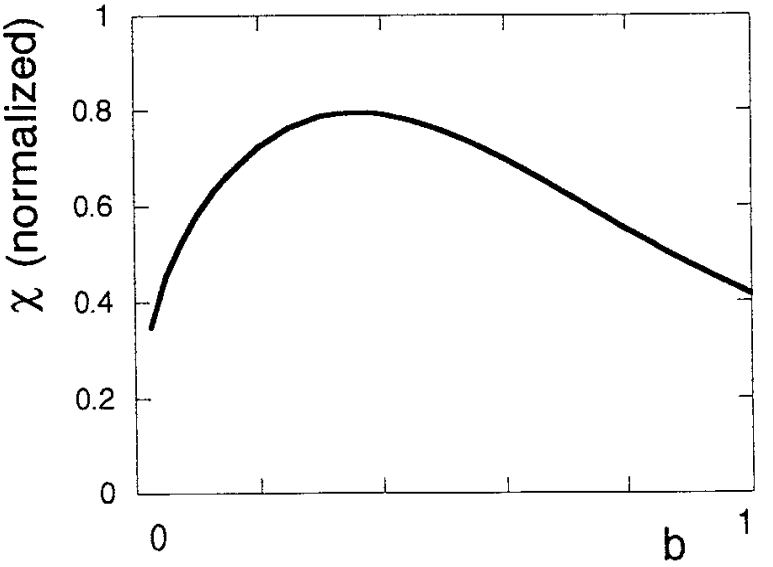
χ (normalized)
1
0.8
0.6
0.4
0.2
0
0
b
1

(b)

Fig. 2

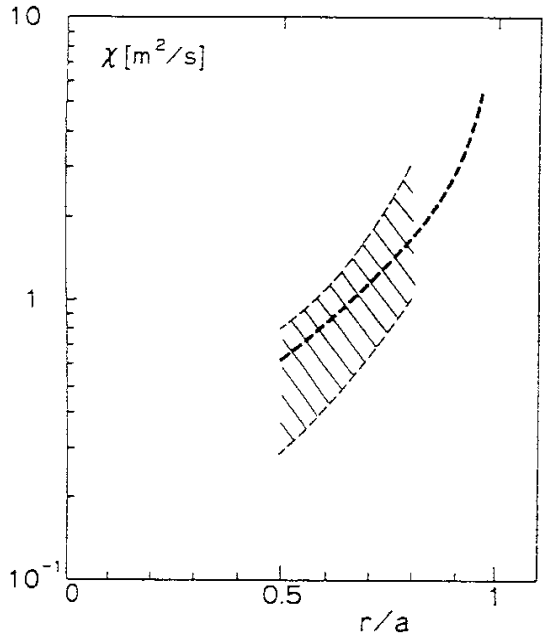

Fig. 3

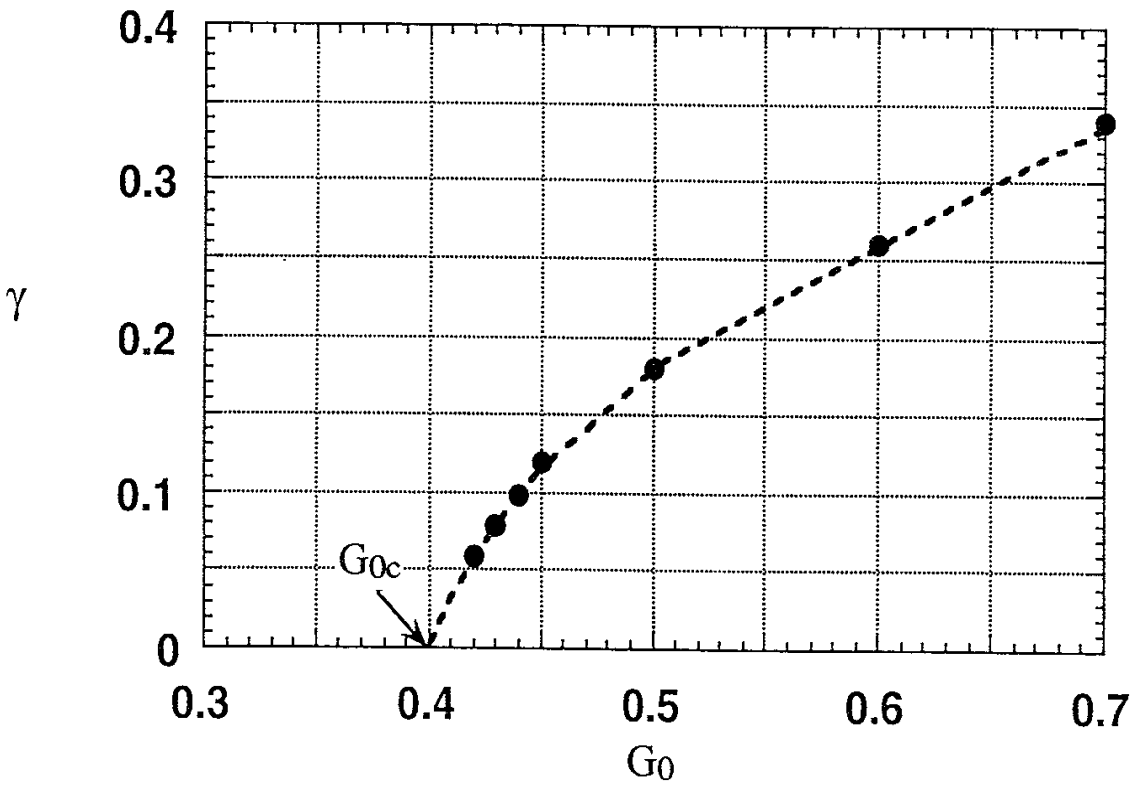

Fig. 4

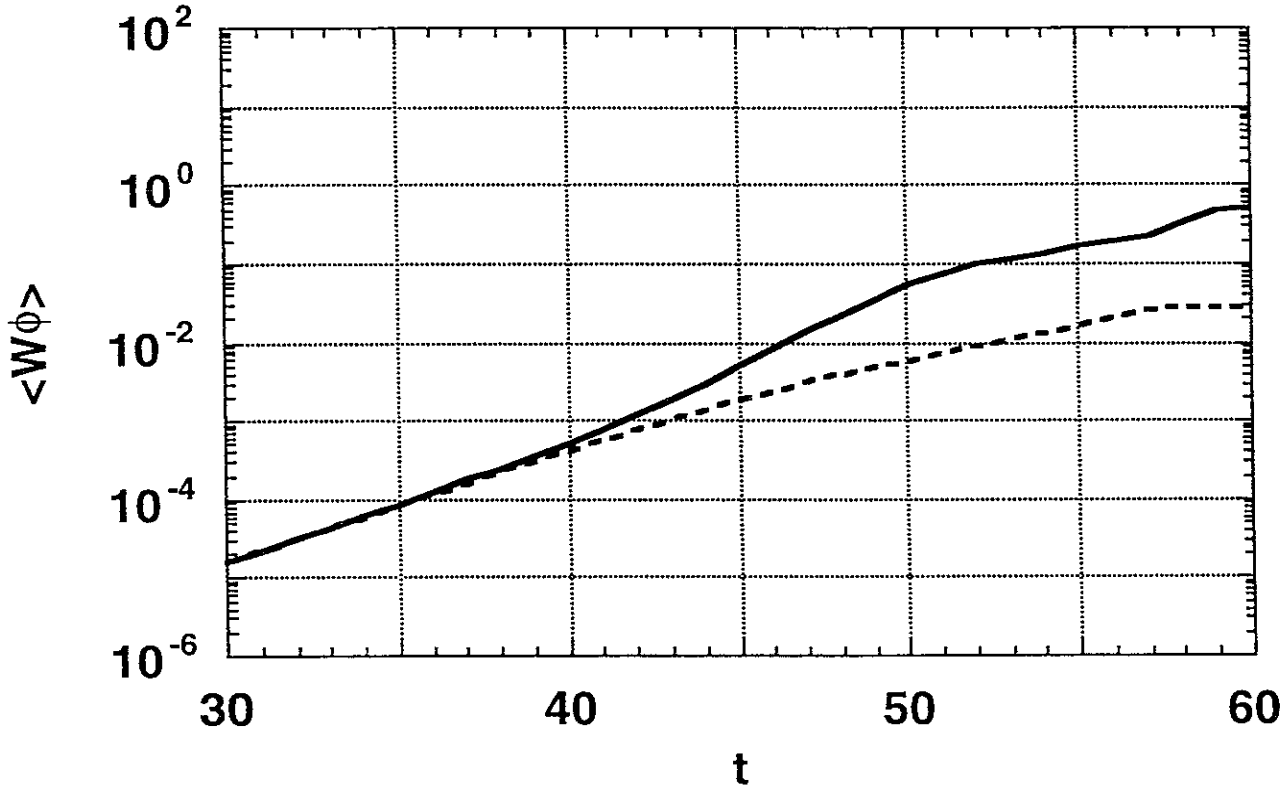
10^2
10^0
10^{-2}
10^{-4}
10^{-6}
<Wϕ>
30
40
50
60
t

Fig. 5

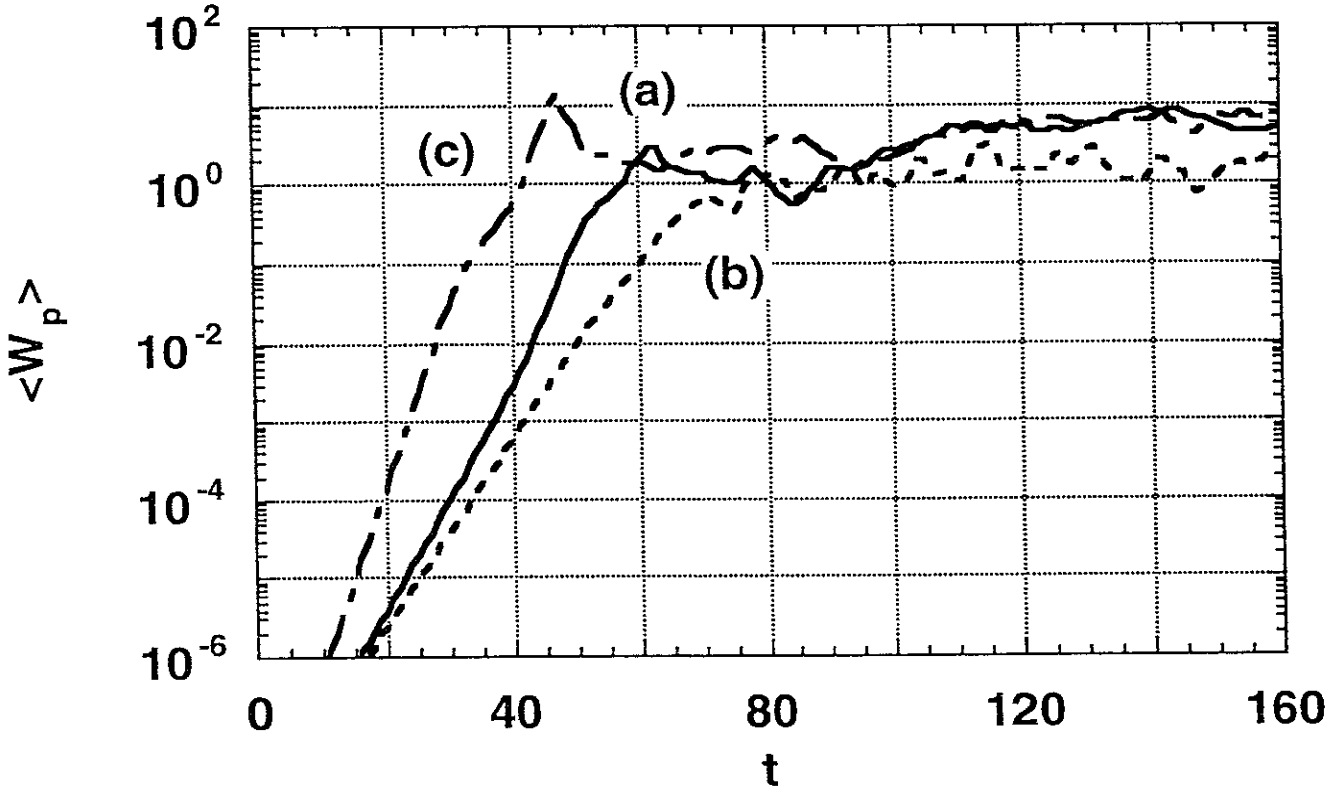
10^2
10^0
10^{-2}
10^{-4}
10^{-6}
<W_p>
(a)
(b)
(c)
0
40
80
120
160
t

Fig. 6

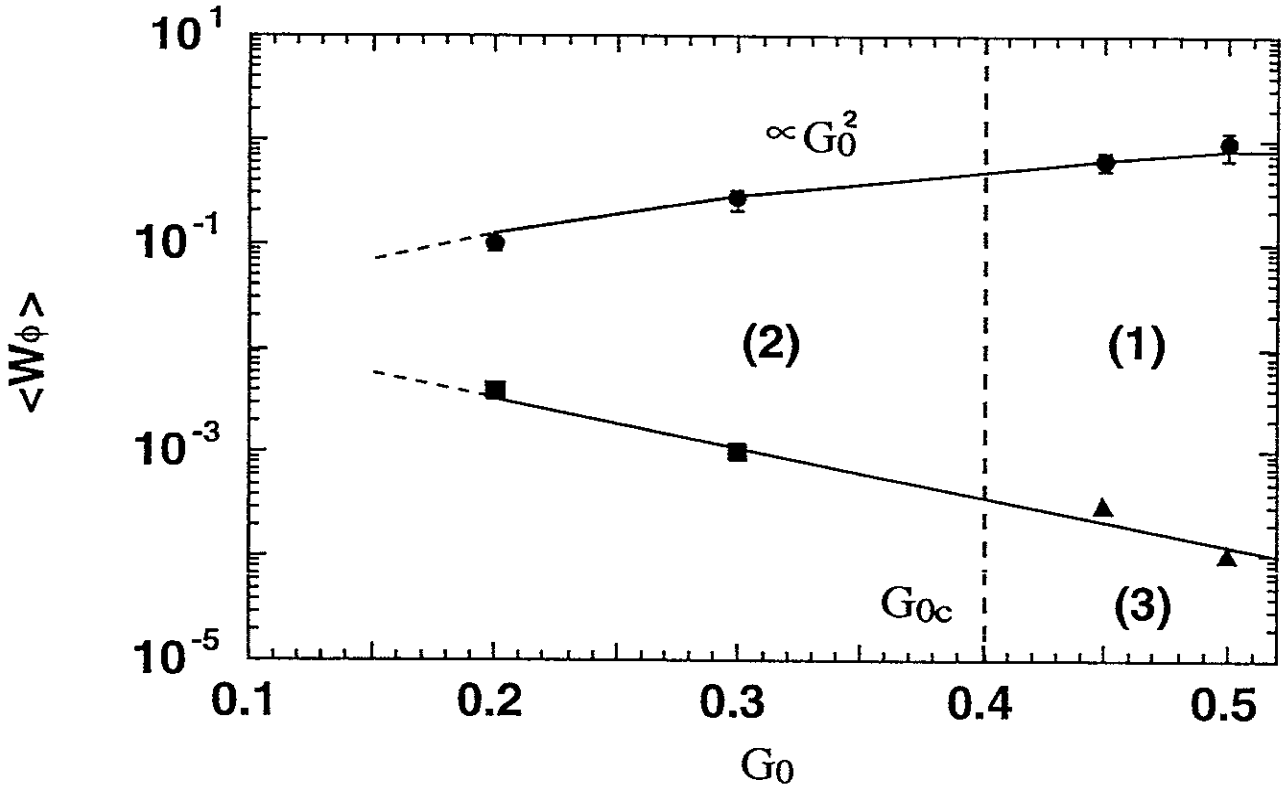
10^{1}
10^{-1}
10^{-3}
10^{-5}
<Wφ>
$\propto G_0^2$
(2)
(1)
(3)
G_{0c}
0.1
0.2
0.3
0.4
0.5
G_0

Fig. 7

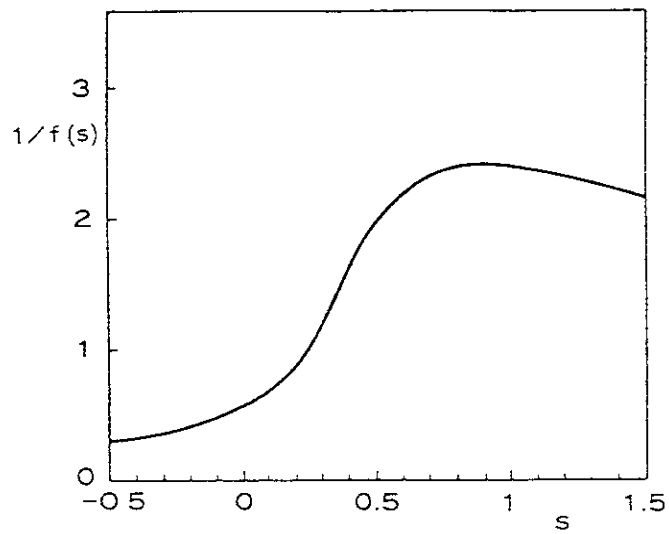
3
1/f(s)
2
1
0
−0.5
0
0.5
1
1.5
s

Fig. 8

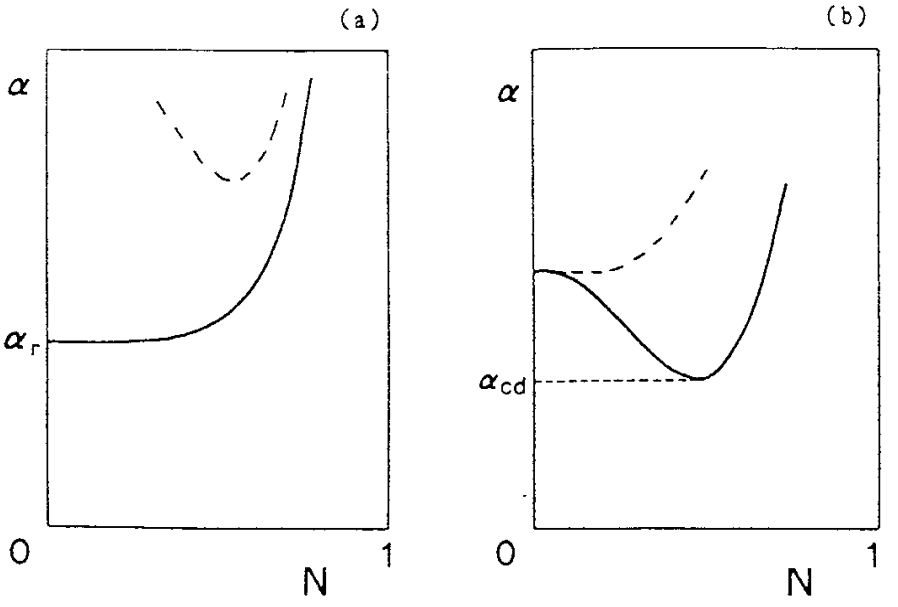
(a)
(b)
α
α
α_r
α_cd
0
1
N
0
1
N

Fig. 9

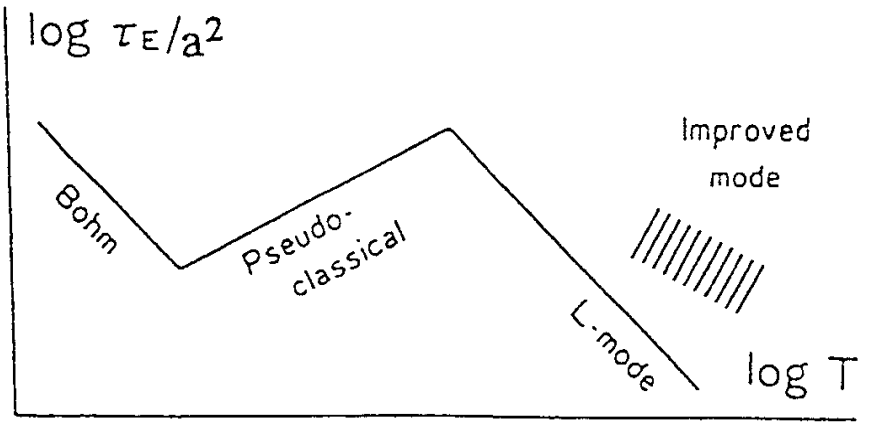
log τ_E/a²
Bohm
Pseudo-
classical
L-mode
Improved
mode
log T

Fig. 10

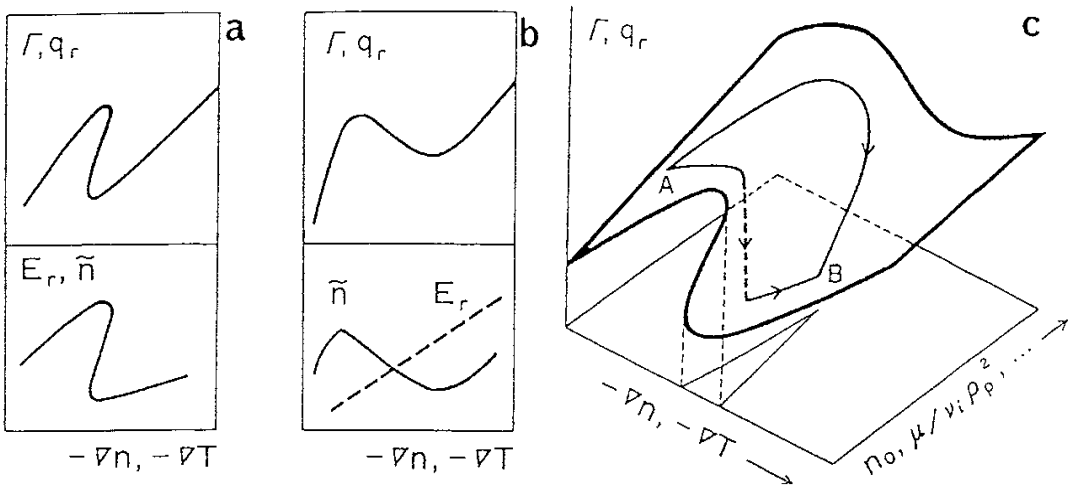
a
Γ, q_r
E_r, ñ
−∇n, −∇T
b
Γ, q_r
ñ
E_r
−∇n, −∇T
c
Γ, q_r
A
B
−∇n, −∇T
n₀, μ/ν_i ρ_p², ...

Fig. 11

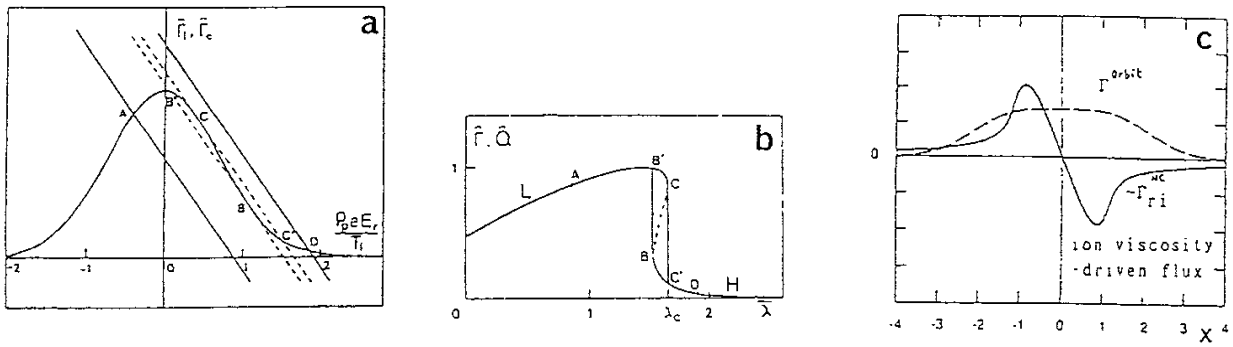
a
Γ̃_i, Γ̃_e
A
B
C
D
ρ_p e E_r / T_i
b
Γ̃, Q̃
L
A
B'
C
B
C'
D
H
λ_c
λ
c
Γ^orbit
−Γ^NC_ri
ion viscosity
-driven flux
x

Fig. 12

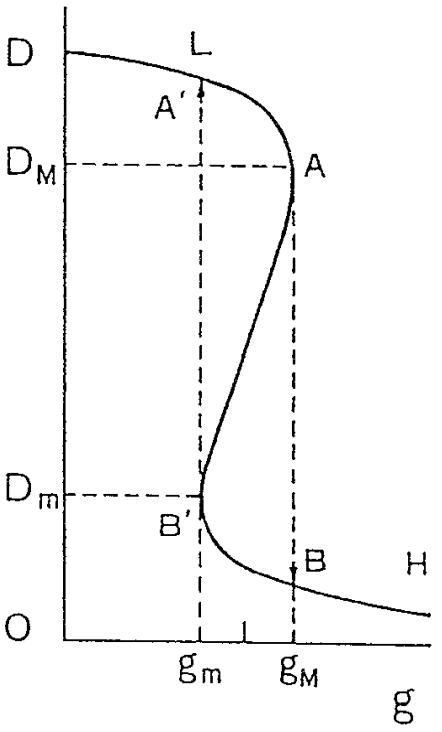

Fig. 13

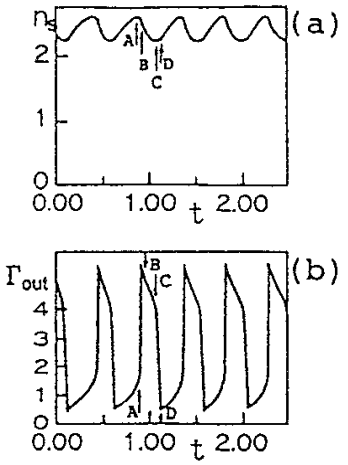

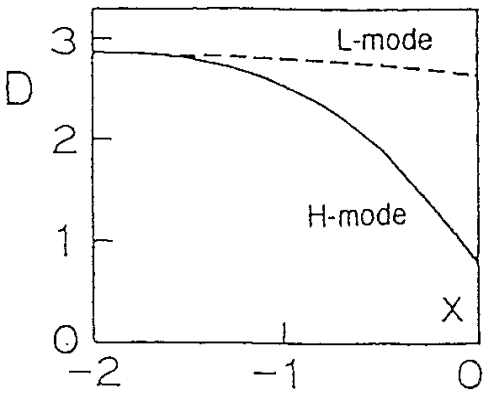

(c)

Fig. 14

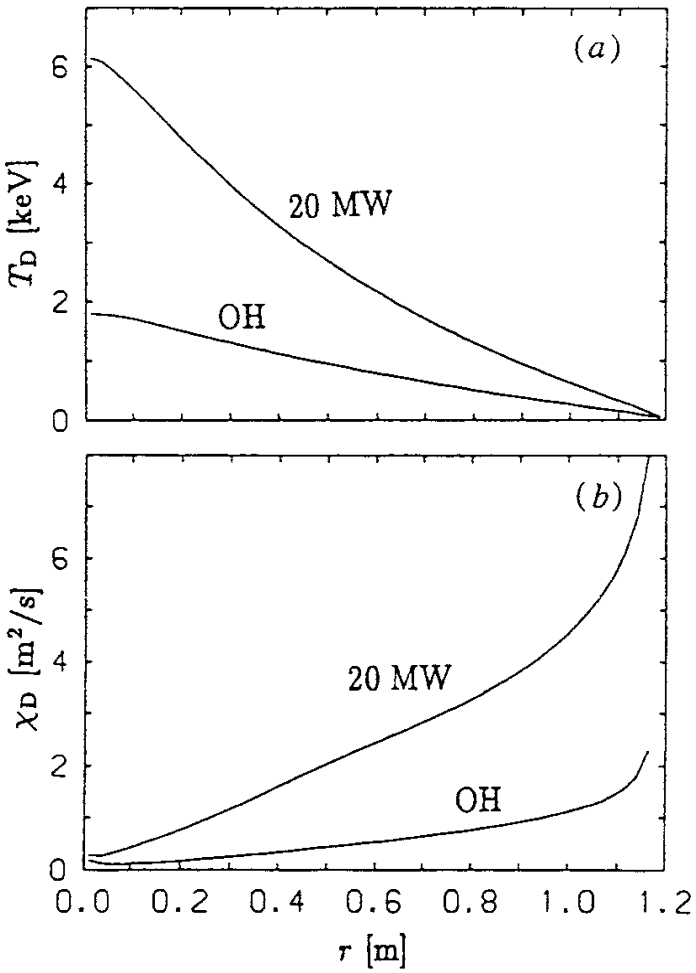
(a)
T_D [keV]
20 MW
OH
(b)
χ_D [m^2/s]
20 MW
OH
r [m]

Fig. 15

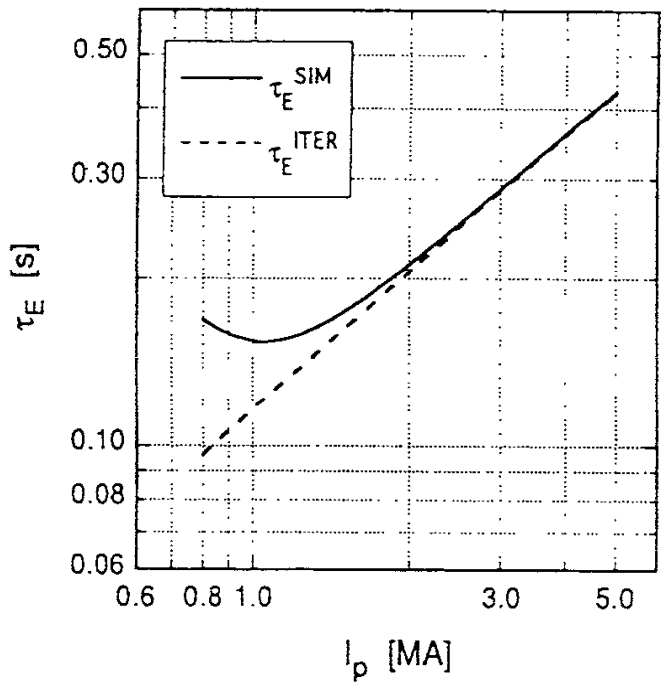
τ_E^{SIM}
τ_E^{ITER}
τ_E [s]
I_p [MA]

Fig. 16

Fig.17

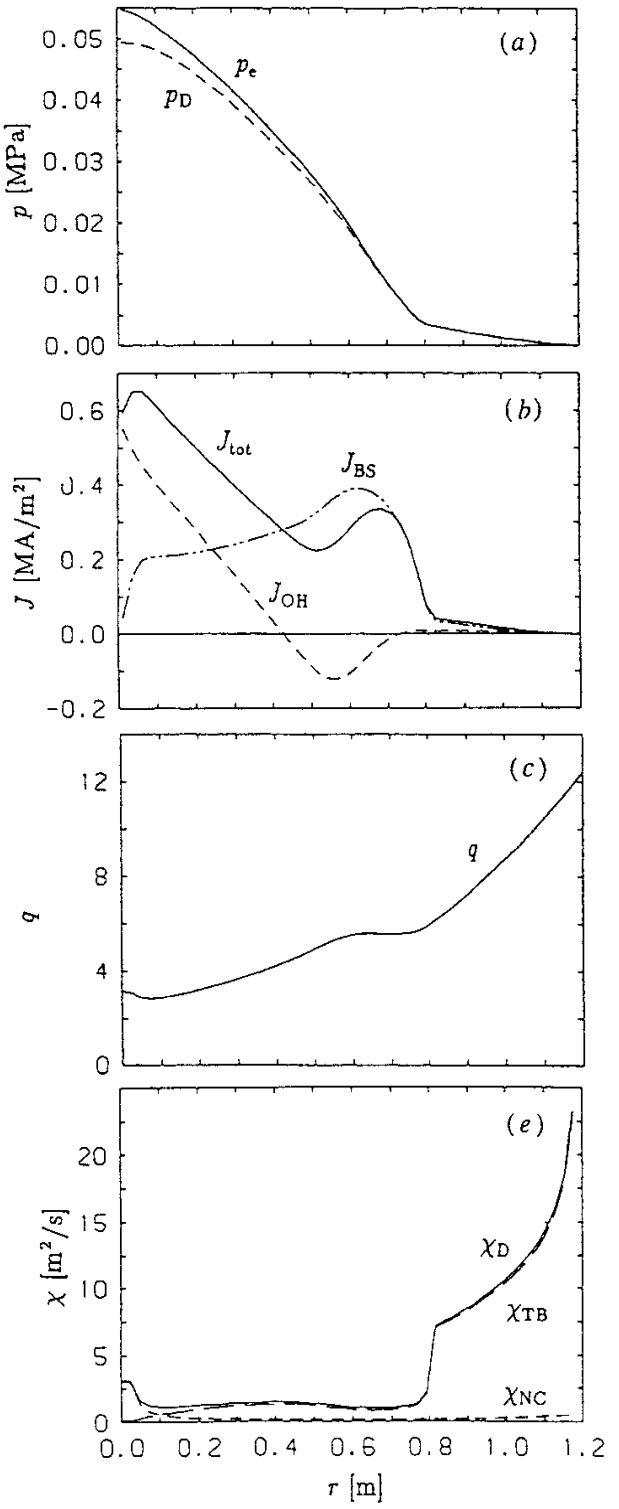
(a)
p_e
p_D
p [MPa]
0.05
0.04
0.03
0.02
0.01
0.00
(b)
J_{tot}
J_{BS}
J_{OH}
J [MA/m^2]
0.6
0.4
0.2
0.0
-0.2
(c)
q
12
8
4
0
(e)
χ_D
χ_{TB}
χ_{NC}
χ [m^2/s]
20
15
10
5
0
0.0
0.2
0.4
0.6
0.8
1.0
1.2
r [m]

Recent Issues of NIFS Series

NIFS-352 A. Taniike,
Energy Loss Mechanism of a Gold Ion Beam on a Tandem Acceleration System: May 1995

NIFS-353 A. Nishizawa, Y. Hamada, Y. Kawasumi and H. Iguchi,
Increase of Lifetime of Thallium Zeolite Ion Source for Single-Ended Accelerator: May 1995

NIFS-354 S. Murakami, N. Nakajima, S. Okamura and M. Okamoto,
Orbital Aspects of Reachable β Value in NBI Heated Heliotron/Torsatrons; May 1995

NIFS-355 H. Sugama and W. Horton,
Neoclassical and Anomalous Transport in Axisymmetric Toroidal Plasmas with Electrostatic Turbulence; May 1995

NIFS-356 N. Ohyabu
A New Boundary Control Scheme for Simultaneous Achievement of H-mode and Radiative Cooling (SHC Boundary); May 1995

NIFS-357 Y. Hamada, K.N. Sato, H. Sakakita, A. Nishizawa, Y. Kawasumi, R. Liang, K. Kawahata, A. Ejiri, K. Toi, K. Narihara, K. Sato, T. Seki, H. Iguchi, A. Fujisawa, K. Adachi, S. Hidekuma, S. Hirokura, K. Ida, M. Kojima, J. Koong, R. Kumazawa, H. Kuramoto, T. Minami,. M. Sasao, T. Tsuzuki, J.Xu, I. Yamada, and T. Watari,
Large Potential Change Induced by Pellet Injection in JIPP T-IIU Tokamak Plasmas; May 1995

NIFS-358 M. Ida and T. Yabe,
Implicit CIP (Cubic-Interpolated Propagation) Method in One Dimension; May 1995

NIFS-359 A. Kageyama, T. Sato and The Complexity Simulation Group,
Computer Has Solved A Historical Puzzle: Generation of Earth's Dipole Field; June 1995

NIFS-360 K. Itoh, S.-I. Itoh, M. Yagi and A. Fukuyama,
Dynamic Structure in Self-Sustained Turbulence; June 1995

NIFS-361 K. Kamada, H. Kinoshita and H. Takahashi,
Anomalous Heat Evolution of Deuteron Implanted Al on Electron Bombardment; June 1995

NIFS-362 V.D. Pustovitov,
Suppression of Pfirsch-schlüter Current by Vertical Magnetic Field in Stellarators; June 1995

NIFS-363 A. Ida, H. Sanuki and J. Todoroki
An Extended K-dV Equation for Nonlinear Magnetosonic Wave in a Multi-Ion Plasma; June 1995

NIFS-364 H. Sugama and W. Horton
Entropy Production and Onsager Symmetry in Neoclassical Transport Processes of Toroidal Plasmas; July 1995

NIFS-365 K. Itoh, S.-I. Itoh, A. Fukuyama and M. Yagi,
On the Minimum Circulating Power of Steady State Tokamaks; July 1995

NIFS-366 K. Itoh and Sanae-I. Itoh,
The Role of Electric Field in Confinement; July 1995

NIFS-367 F. Xiao and T. Yabe,
A Rational Function Based Scheme for Solving Advection Equation; July 1995

NIFS-368 Y. Takeiri, O. Kaneko, Y. Oka, K. Tsumori, E. Asano, R. Akiyama, T. Kawamoto and T. Kuroda,
Multi-Beamlet Focusing of Intense Negative Ion Beams by Aperture Displacement Technique; Aug. 1995

NIFS-369 A. Ando, Y. Takeiri, O. Kaneko, Y. Oka, K. Tsumori, E. Asano, T. Kawamoto, R. Akiyama and T. Kuroda,
Experiments of an Intense H- Ion Beam Acceleration; Aug. 1995

NIFS-370 M. Sasao, A. Taniike, I. Nomura, M. Wada, H. Yamaoka and M. Sato,
Development of Diagnostic Beams for Alpha Particle Measurement on ITER; Aug. 1995

NIFS-371 S. Yamaguchi, J. Yamamoto and O. Motojima;
A New Cable -in conduit Conductor Magnet with Insulated Strands; Sep. 1995

NIFS-372 H. Miura,
Enstrophy Generation in a Shock-Dominated Turbulence; Sep. 1995

NIFS-373 M. Natsir, A. Sagara, K. Tsuzuki, B. Tsuchiya, Y. Hasegawa, O. Motojima,
Control of Discharge Conditions to Reduce Hydrogen Content in Low Z Films Produced with DC Glow; Sep. 1995

NIFS-374 K. Tsuzuki, M. Natsir, N. Inoue, A. Sagara, N. Noda, O. Motojima, T. Mochizuki, I. Fujita, T. Hino and T. Yamashina,
Behavior of Hydrogen Atoms in Boron Films during H_2 and He Glow Discharge and Thermal Desorption; Sep. 1995

NIFS-375 U. Stroth, M. Murakami, R.A. Dory, H. Yamada, S. Okamura, F. Sano and T. Obiki,
Energy Confinement Scaling from the International Stellarator Database; Sep. 1995

NIFS-376 S. Bazdenkov, T. Sato, K. Watanabe and The Complexity Simulation Group,
Multi-Scale Semi-Ideal Magnetohydrodynamics of a Tokamak Plasma; Sep. 1995

NIFS-377 J. Uramoto,
Extraction of Negative Pionlike Particles from a H2 or D2 Gas Discharge Plasma in Magnetic Field; Sep. 1995

NIFS-378 K. Akaishi,
Theoretical Consideration for the Outgassing Characteristics of an Unbaked Vacuum System; Oct. 1995

NIFS-379 H. Shimazu, S. Machida and M. Tanaka,
Macro-Particle Simulation of Collisionless Parallel Shocks; Oct. 1995

NIFS-380 N. Kondo and Y. Kondoh,
Eigenfunction Spectrum Analysis for Self-organization in Dissipative Solitons; Oct. 1995

NIFS-381 Y. Kondoh, M. Yoshizawa, A. Nakano and T. Yabe,
Self-organization of Two-dimensional Incompressible Viscous Flow in a Friction-free Box; Oct. 1995

NIFS-382 Y.N. Nejoh and H. Sanuki,
The Effects of the Beam and Ion Temperatures on Ion-Acoustic Waves in an Electron Beam-Plasma System; Oct. 1995

NIFS-383 K. Ichiguchi, O. Motojima, K. Yamazaki, N. Nakajima and M. Okamoto
Flexibility of LHD Configuration with Multi-Layer Helical Coils; Nov. 1995

NIFS-384 D. Biskamp, E. Schwarz and J.F. Drake,
Two-dimensional Electron Magnetohydrodynamic Turbulence; Nov. 1995

NIFS-385 H. Kitabata, T. Hayashi, T. Sato and Complexity Simulation Group,
Impulsive Nature in Collisional Driven Reconnection; Nov. 1995

NIFS-386 Y. Katoh, T. Muroga, A. Kohyama, R.E. Stoller, C. Namba and O. Motojima,
Rate Theory Modeling of Defect Evolution under Cascade Damage Conditions:The Influence of Vacancy-type Cascade Remnants and Application to the Defect Production Chracterization by Microstructural Analysis; Nov. 1995

NIFS-387 K. Araki, S. Yanase and J. Mizushima,

Symmetry Breaking by Differential Rotation and Saddle-node Bifurcation of the Thermal Convection in a Spherical Shell; Dec. 1995

NIFS-388 V.D. Pustovitov,
Control of Pfirsch-Schlüter Current by External Poloidal Magnetic Field in Conventional Stellarators: Dec. 1995

NIFS-389 K. Akaishi,
On the Outgassing Rate Versus Time Characteristics in the Pump-down of an Unbaked Vacuum System; Dec. 1995

NIFS-390 K.N. Sato, S. Murakami, N. Nakajima, K. Itoh,
Possibility of Simulation Experiments for Fast Particle Physics in Large Helical Device (LHD); Dec. 1995

NIFS-391 W.X.Wang, M. Okamoto, N. Nakajima, S. Murakami and N. Ohyabu,
A Monte Carlo Simulation Model for the Steady-State Plasma in the Scrape-off Layer; Dec. 1995

NIFS-392 Shao-ping Zhu, R. Horiuchi, T. Sato and The Complexity Simulation Group,
Self-organization Process of a Magnetohydrodynamic Plasma in the Presence of Thermal Conduction; Dec. 1995

NIFS-393 M. Ozaki, T. Sato, R. Horiuchi and the Complexity Simulation Group
Electromagnetic Instability and Anomalous Resistivity in a Magnetic Neutral Sheet; Dec. 1995

NIFS-394 K. Itoh, S.-I Itoh, M. Yagi and A. Fukuyama,
Subcritical Excitation of Plasma Turbulence; Jan. 1996

NIFS-395 H. Sugama and M. Okamoto, W. Horton and M. Wakatani,
Transport Processes and Entropy Production in Toroidal Plasmas with Gyrokinetic Eletromagnetic Turbulence; Jan. 1996

NIFS-396 T. Kato, T. Fujiwara and Y. Hanaoka,
X-ray Spectral Analysis of Yohkoh BCS Data on Sep. 6 1992 Flares - Blue Shift Component and Ion Abundances -; Feb. 1996

NIFS-397 H. Kuramoto, N. Hiraki, S. Moriyama, K. Toi, K. Sato, K. Narihara, A. Ejiri, T. Seki and JIPP T-IIU Group,
Measurement of the Poloidal Magnetic Field Profile with High Time Resolution Zeeman Polarimeter in the JIPP T-IIU Tokamak; Feb. 1996

NIFS-398 J.F. Wang, T. Amano, Y. Ogawa, N. Inoue,
Simulation of Burning Plasma Dynamics in ITER; Feb. 1996

NIFS-399 K. Itoh, S-I. Itoh, A. Fukuyama and M. Yagi,
Theory of Self-Sustained Turbulence in Confined Plasmas; Feb. 1996